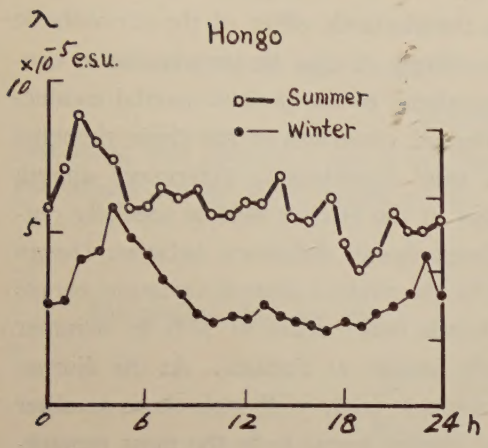


Fig. 4 The diurnal variation curves of the conductivity at Hongo.

variation curve is broken and irregular having the maximum at about 17 L.M.T.. The conductivity curves show less seasonal difference. They are almost regular throughout the year, but the times of maximum and minimum change somewhat occuring at 02 h during the hot season and at about 03 h during the cold season respectively.

The diurnal variation of space charge seems to be not correlated with that of the electric field and conductivity. But, the diurnal variation curve of space charge has its own characteristic, and its maximum value occures at about 8 h L.M.T. throughout the year.

Table 1 *Atmospheric electric field* (unit: V/m)

| time / month | 1 | 2 | 3 | 4 | 5 | 6 | 7 | 8 | 9 | 10 | 11 | 12 |
|---|---|---|---|---|---|---|---|---|---|---|---|---|
| Jan. | 99 | 100 | 100 | 115 | 120 | 135 | 142 | 210 | 270 | 255 | 220 | 200 |
| Feb. | 106 | 106 | 107 | 112 | 102 | 140 | 146 | 162 | 230 | 270 | 230 | 190 |
| Mar. | 85 | 775 | 70 | 90 | 125 | 139 | 140 | 190 | 225 | 260 | 235 | 195 |
| Apr. | 70 | 55 | 60 | 60 | 85 | 100 | 130 | 170 | 200 | 220 | 190 | 170 |
| May | 55 | 50 | 50 | 60 | 80 | 100 | 120 | 150 | 175 | 210 | 200 | 185 |
| June | 41 | 55 | 100 | 137 | 128 | 167 | 159 | 200 | 186 | 194 | 239 | 155 |
| July | 133 | 139 | 120 | 110 | 113 | 129 | 150 | 130 | 143 | 129 | 122 | 191 |
| Aug. | 84 | 76 | 52 | 53 | 60 | 70 | 98 | 90 | 113 | 124 | 118 | 134 |
| Sept. | 40 | 30 | 41 | 47 | 67 | 79 | 79 | 131 | 123 | 136 | 132 | 132 |
| Oct. | 71 | 77 | 70 | 73 | 77 | 89 | 103 | 120 | 156 | 234 | 210 | 210 |
| Nov. | 143 | 133 | 114 | 120 | 156 | 148 | 194 | 200 | 220 | 230 | 260 | 228 |
| Dec. | 110 | 100 | 90 | 115 | 120 | 175 | 180 | 220 | 250 | 300 | 270 | 240 |

| 13 | 14 | 15 | 16 | 17 | 18 | 19 | 20 | 21 | 22 | 23 | 24 |
|---|---|---|---|---|---|---|---|---|---|---|---|
| 170 | 150 | 150 | 170 | 170 | 175 | 180 | 170 | 160 | 150 | 140 | 130 |
| 170 | 164 | 184 | 204 | 199 | 174 | 190 | 183 | 172 | 169 | 157 | 145 |
| 100 | 170 | 165 | 155 | 170 | 190 | 190 | 160 | 140 | 130 | 100 | 95 |
| 140 | 125 | 135 | 130 | 120 | 120 | 130 | 110 | 105 | 90 | 75 | 80 |
| 130 | 125 | 120 | 120 | 130 | 140 | 145 | 120 | 115 | 80 | 80 | 65 |
| 144 | 126 | 159 | 169 | 167 | 198 | 140 | 126 | 119 | 114 | 92 | 84 |
| 170 | 180 | 162 | 194 | 197 | 180 | 118 | 106 | 109 | 117 | 101 | 118 |
| 134 | 207 | 190 | 177 | 176 | 160 | 102 | 99 | 92 | 92 | 75 | 67 |
| 138 | 120 | 106 | 114 | 110 | 103 | 95 | 63 | 76 | 70 | 90 | 44 |
| 178 | 180 | 159 | 176 | 170 | 167 | 135 | 130 | 73 | 87 | 65 | 80 |
| 211 | 180 | 215 | 220 | 245 | 260 | 230 | 198 | 210 | 173 | 160 | 176 |
| 200 | 190 | 170 | 175 | 180 | 190 | 170 | 160 | 145 | 140 | 135 | 130 |

The partial conductivity observed at Hongo was the only positive one. So long as the electric field is less than about 300 V/m, the electrode effect of the atmospheric electric field seems not to be so effective. Accordingly, it may be permissible to consider that the total electric conductivity is proportional to the positive partial conductivity in the stationary state. Comparing the diurnal variations of the three elements obtained in various seasons of the year, there exist considerable differences among them both in magnitude and characters, and that of the electric field is specially outstanding in the grade of difference. The most remarkable difference between Hongo and Tanashi [6], [7], [8] is the seasonal change of the mode of diurnal variation curves of the electric field. The maximum value of electric field occurs at 17 h in summer and 10 h in winter at Hongo, and 8 h in both seasons at Tanashi. As the diurnal variation curves of the electric field at Tanashi coincide fairly well with those at other stations situated in rural condition, the seasonal change seems to be the most remarkable characteristic at Hongo situated in urban condition.

### 3. Fundamental equations

The atmospheric electric field in the stationary state may be described by the equations.

$$\nabla \times \boldsymbol{H} = \boldsymbol{i} \tag{1}$$

$$\nabla \times \boldsymbol{E} = 0 \tag{2}$$

$$\nabla \cdot \boldsymbol{B} = 0 \tag{3}$$

$$\nabla \cdot \boldsymbol{D} = \rho \tag{4}$$

Since the conduction current by the large ion is negligible small, the conduction current in the atmospheric electric field seems to depend only upon the small ion. So, we may assume the following relation:

$$\boldsymbol{i} = \lambda \boldsymbol{E} \tag{5}$$

Further, we shall assume that

$$\boldsymbol{D} = \varepsilon \boldsymbol{E} \tag{6}$$

Putting (6) into (4), we get

$$\nabla \cdot (\varepsilon \boldsymbol{E}) = \rho \tag{7}$$

It follows from (2) that

$$\nabla \cdot \boldsymbol{i} = 0 \tag{8}$$

Then, from (5) and (8), we have

$$\nabla \cdot (\lambda \boldsymbol{E}) = 0 \tag{9}$$

Referring to (7), we get

$$\nabla \cdot (\varepsilon \boldsymbol{E}) = \nabla \cdot \left( \frac{\varepsilon}{\lambda} \lambda \boldsymbol{E} \right) = \lambda \boldsymbol{E} \cdot \nabla \left( \frac{\varepsilon}{\lambda} \right) + \frac{\varepsilon}{\lambda} \nabla \cdot (\lambda \boldsymbol{E}) = \rho \tag{10}$$

Substituting (5) into (10), we get

$$\boldsymbol{E} \cdot \nabla \left( \frac{\varepsilon}{\lambda} \right) = \frac{\rho}{\lambda} \tag{11}$$

From (11), we get

$$\boldsymbol{E} \cdot \nabla (\log \lambda) = -\frac{\rho}{\varepsilon} \tag{12}$$

From (2), we get

$$\boldsymbol{E}=-\nabla\phi \tag{13}$$

Putting (13) into (9), we have

$$\nabla\cdot(\lambda\nabla\phi)=0 \tag{14}$$

Assuming that both of $\lambda$ and $\phi$ are functions of the radial component of the spherical coordinate, we get from equation (14):

$$\frac{1}{r^2}\frac{d}{dr}\left(r^2\lambda\frac{d}{dr}\phi\right)=0 \tag{15}$$

Integrating (15), we get

$$\frac{d}{dr}\phi=\frac{C}{\lambda(r)r^2} \tag{16}$$

$\boldsymbol{E}=\boldsymbol{n}_r E_r$; $\boldsymbol{n}_r$: unit vector

$$E_r=-\frac{d}{dr}\phi=-\frac{C}{\lambda(r)r^2} \tag{17}$$

Total current $I$ can be given by the following relation:

$$I=\int_0^{2\pi}d\varphi\int_0^{\pi}(\boldsymbol{i}\cdot\boldsymbol{n}_r)\,r^2\sin\theta\,d\theta \tag{18}$$

Here,

$$\boldsymbol{i}=\lambda\boldsymbol{E}=-\boldsymbol{n}_r\frac{C}{r^2} \tag{19}$$

From (18) and (19), we get

$$I=\int_0^{2\pi}d\varphi\int_0^{\pi}\lambda E_r r^2\sin\theta\,d\theta=-4\pi C \tag{20},\qquad \therefore\quad C=-\frac{I}{4\pi} \tag{21}$$

Putting (21) into (17) and (19), we get

$$\boldsymbol{i}=\boldsymbol{n}_r\frac{I}{4\pi r^2},\quad \boldsymbol{E}=\boldsymbol{n}_r\frac{I}{4\pi\lambda r^2} \tag{22}$$

Substituting (22) into (7), we get as follows.

$$\rho=\varepsilon\frac{1}{r^2}\frac{d}{dr}\left(r^2\frac{I}{4\pi r^2\lambda}\right)=\frac{\varepsilon I}{4\pi r^2}\frac{d}{dr}\left(\frac{1}{\lambda}\right) \tag{23}$$

Here, $4\pi r^2$ is the total surface area of the earth. Accordingly, $I/(4\pi r^2)$ is equal to the conduction current density at the earth's surface and will be expressed by the symbol $i$ hereafter. Considering the small area of the earth's surface, and assuming $\varepsilon$ being 1 in the air, we can write the formula (23) as follows:

$$\rho=i\frac{d}{dz}\left(\frac{1}{\lambda}\right) \tag{24}$$

Where $z$ is the vertical axis of the orthogonal coordinate. Using the electrostatic unit, we can write (24) as follows.

$$\rho=\frac{i}{4\pi}\frac{d}{dz}\left(\frac{1}{\lambda}\right) \tag{24'}$$

The formula (24') gives the relation among the space charge, conduction current density and the vertical distribution of the air-resistivity.

## 4. The vertical distribution of the electrical conductivity of the atmosphere near the ground

Taking into account the influence of the eddy diffusion, we may describe the process of the ionization equilibrium by the following equation.

$$K\frac{d^2n}{dz^2}+q=\alpha n^2+\beta Nn \tag{25}$$

Here, $K$, $\alpha$ and $\beta$ are the coefficient of eddy diffusivity, coefficient of recombination of the small ion and the coefficient of attachment between the small ion and nuclei respectively. And, $q$, $n$ and $N$ are the rate of ion pair production, small ion number and nuclei content respectively. The left hand of equation (25) expresses the sum of the net flux of ions due to the eddy diffusion and the rate of ion pair production by the all kind of ionization in the reference volume, and the right hand expresses the sum of the rate of ion destruction by recombination and attachment in the same volume.

Over land, especially near centres of pollution, the values of $N$ are often observed so large that the first term of right hand side of (25) can be ignored compared to the second. In these cases, the equation (25) may be written as follows.

$$K\frac{d^2n}{dz^2}+q=\beta Nn \tag{25'}$$

The ionizing agents of the atmosphere near the ground are as follows:

i) Radiation by the radioactive gases and their decay products in the atmosphere.

ii) Penetrating radiation by the radioactive subtances in the earth's crust.

iii) Cosmic ray.

Considering that the quantities of radiation of cosmic ray and penetrating radiation from the earth's crust are not affected by air motions, we may say that the rate of ion pair production by these two ionizing agents are independent of air motions. On the other hand, the distribution of the radioactive gases and their decay products in the atmosphere are affected directly by air motions as discussed in the previous paper (9). Therefore the rate of ion pair production by the radiation from these substances is influenced by air motions. Then, we may classify these three ionizing agents into two groups:

i) Radiation by the radioactive gases and their decay products in the atmosphere, which is affected by air motions.

ii) Penetrating radiations by the radioactive substances in the earth's crust and cosmic ray, which are not affected by air motions.

Let us denote by $q_1$ and $q_2$ the rates of ion pair production by the ionizing agents i) and ii) respectively. Then, we may write as follows:

$$q=q_1+q_2 \tag{26}$$

Assuming that the vertical distribution of the radioactive substance in the atmosphere is controlled by the eddy diffusivity, the distribution of the substance is expressed by the following formula. Here, $\tau$ and $K$ are the decay constant of Rn and the coefficient of eddy diffusivity respectively.

$$Q=Q_h e^{-\sqrt{\tau/K}\cdot(z-h)} \tag{27}$$

The ionization due to the radioactive substances in the atmosphere is mainly caused by $\alpha$ rays. Consequently, the rate of ion pair production, due to the radiation by the radioactive substances in the atmosphere, may be considered to be proportional to the content of the radioactive substances in the atmosphere.
In other word, we may write:

$$q_1=k_1 Q \tag{28}$$

where $k_1$ is a constant.

Substituting (28) into (27), we get the following formula·

$$q_1=q_{1h}\, e^{-\sqrt{\tau/K}\cdot(z-h)} \tag{29}$$

where $q_{1h}$ is the value of the rate of ion pair production at $z=h$.
Then, $q$ is given by

$$q=q_{1h}\, e^{-\sqrt{\tau/K}\cdot(z-h)}+q_2 \tag{30}$$

Referring to (25′), the equation form becomes

$$K\frac{d^2n}{dz^2}+q_{1h}\, e^{-\sqrt{\tau/K}\cdot(z-h)}+q_2=\beta N n \tag{31}$$

Boundary conditions for $n$ are

$$n=n_h \qquad \text{at} \quad z=h$$

$$n: \text{finite} \qquad \text{at} \quad z=\infty$$

The solution of equation (31) is found to be that:

$$n=\left\{n_h-\left(\frac{q_{1h}}{\beta N-\tau}+\frac{q_2}{\beta N}\right)\right\}e^{-\sqrt{\beta N/K}\cdot(z-h)}+\frac{q_{1h}}{\beta N-\tau}e^{-\sqrt{\tau/K}\cdot(z-h)}+\frac{q_2}{\beta N} \tag{32}$$

The vertical distribution of the electrical conductivity of the atmosphere near the ground is given by the following formula.

$$\lambda=nek=\left[\left\{n_h-\left(\frac{q_{1h}}{\beta N-\tau}+\frac{q_2}{\beta N}\right)\right\}e^{-\sqrt{\beta N/K}\cdot(z-h)}+\frac{q_{1h}}{\beta N-\tau}e^{-\sqrt{\tau/K}\cdot(z-h)}+\frac{q_2}{\beta N}\right]ek \tag{33}$$

Where $k$ is the mobility of small ion, and assumed to be constant. Accordingly, the vertical distribution of the air resistivity near the ground is given by the following formula.

$$r=1\Big/\left[\left\{n_h-\left(\frac{q_{1h}}{\beta N-\tau}+\frac{q_2}{\beta N}\right)\right\}e^{-\sqrt{\beta N/K}\cdot(z-h)}+\frac{q_{1h}}{\beta N-\tau}e^{-\sqrt{\tau/K}\cdot(z-h)}+\frac{q_2}{\beta N}\right]ek \tag{34}$$

## 5. The relation between the atmospheric electric field and the other elements near the ground

Differentiating the formula (34), we get

$$\frac{dr}{dz}=\frac{\left(\frac{\beta N}{K}\right)^{1/2}\left\{n_h-\left(\frac{q_{1h}}{\beta N-\tau}+\frac{q_2}{\beta N}\right)\right\}e^{-\sqrt{\beta N/K}\cdot(z-h)}+\left(\frac{\tau}{K}\right)^{1/2}\frac{q_{1h}}{\beta N-\tau}e^{-\sqrt{\tau/K}\cdot(z-h)}}{\left[\left\{n_h-\left(\frac{q_{1h}}{\beta N-\tau}+\frac{q_2}{\beta N}\right)\right\}e^{-\sqrt{\beta N/K}\cdot(z-h)}+\frac{q_{1h}}{\beta N-\tau}e^{-\sqrt{\tau/K}\cdot(z-h)}+\frac{q_2}{\beta N}\right]^2 ek} \tag{35}$$

Substituting (35) into (24′), we get the following formula.

$$\rho=\frac{i}{4\pi}\frac{\left(\frac{\beta N}{K}\right)^{1/2}\left\{n_h-\left(\frac{q_{1h}}{\beta N-\tau}+\frac{q_2}{\beta N}\right)\right\}e^{-\sqrt{\beta N/K}\cdot(z-h)}+\left(\frac{\tau}{K}\right)^{1/2}\frac{q_{1h}}{\beta N-\tau}e^{-\sqrt{\tau/K}\cdot(z-h)}}{\left[\left\{n_h-\left(\frac{q_{1h}}{\beta N-\tau}+\frac{q_2}{\beta N}\right)\right\}e^{-\sqrt{\beta N/K}\cdot(z-h)}+\frac{q_{1h}}{\beta N-\tau}e^{-\sqrt{\tau/K}\cdot(z-h)}+\frac{q_2}{\beta N}\right]^2 ek}$$

$$=\frac{n_hE}{4\pi}\frac{\left(\frac{\beta N}{K}\right)^{1/2}\left\{n_h-\left(\frac{q_{1h}}{\beta N-\tau}+\frac{q_2}{\beta N}\right)\right\}e^{-\sqrt{\beta N/K}\cdot(z-h)}+\left(\frac{\tau}{K}\right)^{1/2}\frac{q_{1h}}{\beta N-\tau}e^{-\sqrt{\tau/K}\cdot(z-h)}}{\left[\left\{n_h-\left(\frac{q_{1h}}{\beta N-\tau}+\frac{q_2}{\beta N}\right)\right\}e^{-\sqrt{\beta N/K}\cdot(z-h)}+\frac{q_{1h}}{\beta N-\tau}e^{-\sqrt{\tau/K}\cdot(z-h)}+\frac{q_2}{\beta N}\right]^2} \tag{36}$$

At height $h$, this relation becomes

$$\rho_h=\frac{n_hE_h}{4\pi}\frac{\left(\frac{\beta N}{K}\right)^{1/2}\left\{n_h-\left(\frac{q_{1h}}{\beta N-\tau}+\frac{q_2}{\beta N}\right)\right\}+\left(\frac{\tau}{K}\right)^{1/2}\frac{q_{1h}}{\beta N-\tau}}{n_h^2}$$

$$=\frac{E_h}{4\pi}\frac{\left(\frac{\beta N}{K}\right)^{1/2}\left\{n_h-\left(\frac{q_{1h}}{\beta N-\tau}+\frac{q_2}{\beta N}\right)\right\}+\left(\frac{\tau}{K}\right)^{1/2}\frac{q_{1h}}{\beta N-\tau}}{n_h} \tag{37}$$

This formula gives the relation among the elements of the atmospheric electricity at height $h$ above the ground.

Considering that the value of $\tau$ is $2.09\times10^{-6}$sec.$^{-1}$, and that of $\beta N$ is nearly $10^{-2}$ sec.$^{-1}$ on land, (37) may be reduced to

$$\rho_h=\frac{E_h}{4\pi}\frac{\left(\frac{\beta N}{K}\right)^{1/2}\left(n_h-\frac{q_{1h}+q_2}{\beta N}\right)}{n_h} \tag{38}$$

From (38), we get

$$E_h=4\pi\rho_h\frac{n_hK^{1/2}}{(\beta N)^{1/2}\left(n_h-\frac{q_{1h}+q_2}{\beta N}\right)} \tag{39}$$

The formula (39) expresses the electric field considering the influence of the eddy diffusion on the vertical distribution of the electrical conductivity of the atmosphere. The formula (39) is rewritten as

$$N=\frac{1}{\beta}\left[\left(\frac{q_{1h}+q_2}{n_h}\right)^{1/2}+\frac{2\pi\rho_h}{E_h}K^{1/2}+\frac{1}{2}\left(\frac{q_{1h}+q_2}{n_h}\right)^{-1/2}\left(\frac{2\pi\rho_h}{E_h}\right)^2K\right]^2 \tag{40}$$

This formula gives the nuclei content near the ground. Here, the hourly values of $E_h$, $\rho_h$, $n_h$ are shown in Fig. 2~4. $q_{1h}+q_2$ and $K$ are shown in the other paper (9) (10). The value of $\beta$ employed here, is $5\times10^{-6}$cm$^3$sec$^{-1}$

Using these hourly values and (40), the diurnal variation of the nuclei content can be computed. The results are shown in Fig. 5 for summer and winter seasons. As we can see in this figure, the calculated values of the nuclei content are 8,000 –14,000 cc$^{-1}$ in summer, and 12,000–22,000 cc$^{-1}$ in winter. The mode of diurnal variation curve in summer is similar to that in winter, and the number of $N$ is large at night and small in the daytime. Although the routin observation of $N$ was not carried out at Hongo, the values observed by Aitken counter at Nishigahara in summer, 1953

were about 10,000 $cc^{-1}$ at night and about 8,000 $cc^{-1}$ in the daytime. We may say that the calculated values coincide fairly well with the observed values. Fig. 6 shows the diurnal variation curve of the dust concentration observed by Koshi (11) at Shiba, Tokyo. In this figure, $Y$ is used for the unit of the dust concentration, and it is almost proportional to the nuclei content. The modes of the computed diurnal variation curves and the seasonal change, shown in Fig. 5, coincide fairly well with observed ones. It appeares the good coincidence that the atmospheric electric field near the ground can be expressed considerably well by the formula (40). Morever, from the results noted above we may say the atmospheric electric field is proportional to the

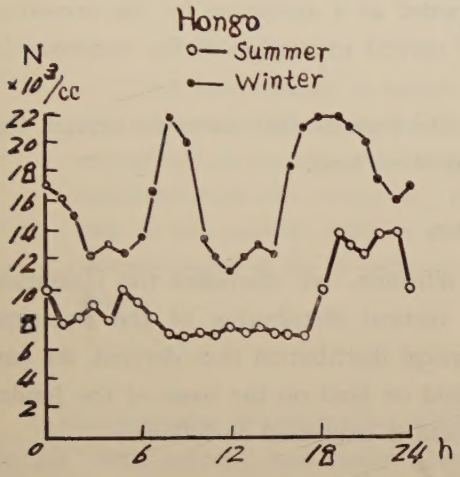


Fig. 5 The estimated diurnal variation curves of the nuclei content at Hongo.

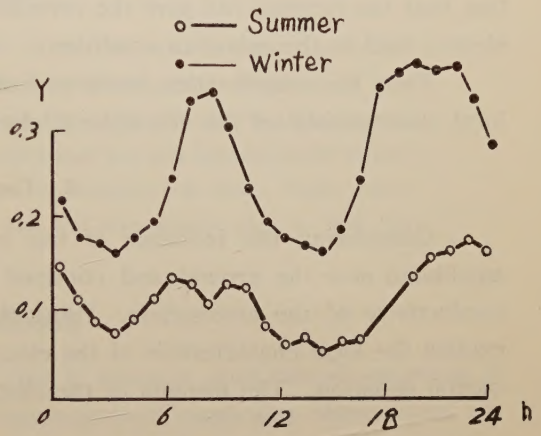


Fig. 6 The observed diurnal variation curves of nuclei content in Tokyo.

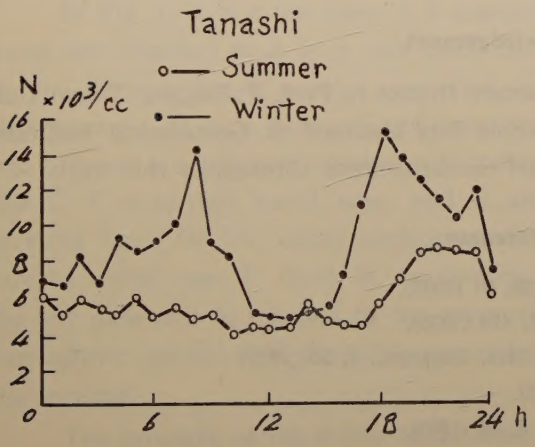


Fig. 7 The estimated diurnal viaration curves of nuclei content at Tanashi.

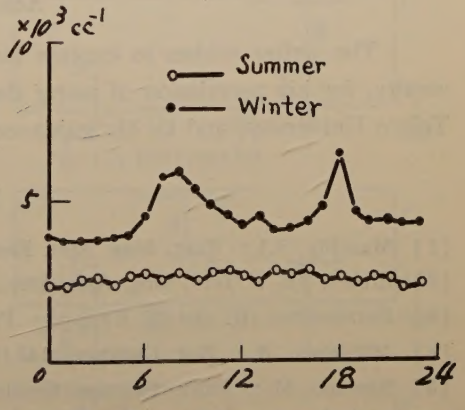


Fig. 8 The observed diurnal variation curves of large ion number at Tanashi.

product of the space charge and the square root of the coefficient of eddy diffusivity. Although the discussions mentioned above are concerned with the atmospheric electric field at Hongo, no generality is lost in the discussion. Consequently, the diurnal variation of the atmospheric electric field in the suburban or rural conditions may be explained

in the same way. In Fig. 7, shown is the diurnal variation of the nuclei content, $N$, for Tanashi, computed from (40). Uses are made of the observed values of the atmospheric electric field, space charge and ion number at Tanashi. [6], [7], [8]

Since the rate of ion pair production by the penetrating radiation from the ground surface is not measured at Tanashi, the value obtained at Hongo is used. Fig. 8 shows the diurnal variation curve of the large ion number observed at Tanashi [12]. According to the results of observations the nuclei content is almost proportional to the large ion number. Consequently, the correspondence between the computed diurnal variation of the nuclei content and the diurnal variation of the large ion number observed in suburban condition may be again regarded as a guarantee for the presumption that the formula (40) give the considerably correct expression of the atmospheric electric field in the suburban condition.

From the consideration mentioned above, the formula (40) seems to explain the local characteristic of the atmospheric electric field on land.

## 6. Conclusion

Considering the influence of the eddy diffusion, we discussed the ionization equilibuim near the ground and obtained the vertical distribution of the electrical conductivity of the atmosphere. Using the vertical distribution thus derived, we can explain the local characteristic of the electric field on land on the basis of the fundamental equation. The formula of the electric field is expressed as follows:

$$E_h = 4\pi\rho_h \frac{n_h K^{1/2}}{(\beta N)^{1/2}\left(n_h - \frac{q_{1h}+q_2}{\beta N}\right)}$$

## Acknowledgement

The writer wishes to express his sincere thanks to Prof. T. Nagata, Tokyo University, for his permission of using the whole data obtained at Geophysical Institute, Tokyo University, and to his guidance and encouragement throughout this work.

## References

[1] Mauchly, S.J.: Terr. Mag. Atm. Elec.. **28**, 61 (1923).
[2] Brown, J.G.: Terr. Mag. Atm. Elec., **40**, 413 (1935).
[3] Hatakeyama, H. and M. Kawano: Pap. Met. Geophys., **4**, 55 (1935).
[4] Mühleisen, R.: Zeit. Geophys., 142 (1953).
[5] Kawano, M.: Journ. Geomag. Geoelec., **5**, 16 (1953).
[6] Aoki, T.: Researches of the Electrotechnical Laboratory, No. 494 (1949).
[7] Aoki, T. and K. Kato: Journ. Electrotechnical Laboratory, **18**, 562 (1954).
[8] Kawasaki, K. and K. Kato: Journ. Electrotechnical Laboratory, **16**, 200 (1952).
[9] Kawano, M.: Journ. Met. Soc. Japan, **35**, No. 6 (1957).
[10] Kawano, M.: Journ. Met. Soc. Japan, **35**, No. 6 (1957).
[11] Koshi, S.: Journ. Met. Soc. Japan, **34**, 327 (1956).
[12] Aoki, T. and K. Kato: Journ. Electrotechnical Laboratory, **17**, 339 (1953).

# Simultaneous Measurements of the Air Earth Current and the Atmospheric Electric Potential Gradient

By Miyoji Goto

*Aso Institute, Kyoto University*

(Read Oct. 11, 1957; Received Nov. 10, 1957)

**Abstract**

The main difficulty in measurements of the air earth current lies in the elimination of displacement current caused by short period variations of the atmospheric electric field. An apparatus free from this difficulty was constructed and observations were carried out. It is ascertained that this apparatus can be well used in fine weather condition as well as in thunderstorm time. Some simultaneous records of the air earth current and the atmospheric electric field are shown.

## 1. Introduction

An apparatus is constructed which is able to measure short period variations of the air earth current, and under various meteorological conditions observations are carried out. In order to eliminate the displacement current caused by field induction the following consideration is taken into account.

In Fig. 1, A is a test plate, C is a small metal disc attached to A by a thin metal rod B, and D is a brush contact connected to electrometer. E is a plate of compensator, which forms a condenser together with metal disc C, F a earthed metal case, and G an earthing key. On the upper surface of the earthed metal case F there is an opening, the test plate can be exposed to the external atmospheric electric field throughly just under the opening.

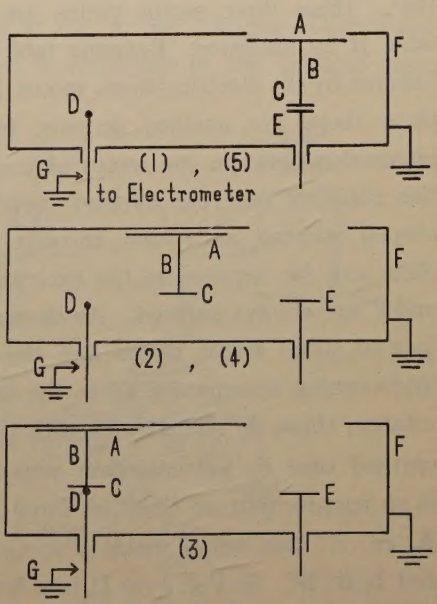


Fig. 1 Working principle of the apparatus

The principle of the action of the apparatus is as follows. In Fig. 1 (1) the insulated test plate system (A.B.C) which is in earth potential at the beginning of the observation, is exposed to atmospheric electric field, then the system receives equal and opposite charges induced by the external field and net charge

by air earth current. In Fig. 1 (2) when this insulated plate system is brought into the earthed case F, and free from the field influence, then induced charges vanish, and only net charge carried by air earth current remaines. In Fig. 1 (3) the insulated system contacts with the electrometer system, a portion of net charge is supplied to it. In Fig. 1 (4) the insulated plate system moves towards the opening. Fig. 1 (5) the insulated system is again exposed to the atmospheric electric field, the system receives induced charge and air earth current again. By the repetition of the above mentioned process, the potential of the test plate system (A.B.C) and the electrometer system rises in turn by charge from the air earth current only. Accordingly the air earth current is able to be measured.

The plate system has a certain potential caused by the field induction when exposed to the external electric field, so that the lines of force above the test plate will be distorted, therefore the incoming air earth current is modified to some extent. In order to keep the plate system at earth potential when exposed to the field, and to make the air earth current enter just as it is, the compensation device similar with the compensator of the universal portable electrometer of C.T.R. Wilson (1905, 1906, 1908) is applied. The electric potential given to E (Fig. 1) is adjusted according to the atmospheric field intensity and automatic compensation is made continually. This device will be described in detail afterwards.

## 2. Apparatus

According to the principle mentioned above the following apparatus is constructed. The test plate which is exposed to the atmospheric electric field is consisted of, as in Fig. 2, three sector plates A, A′, A″, each sector angle is 120°. These three sector plates are fixed on the rotating table H by insulator. Rotating table H has a rotating axis I driven by the electric phono motor J. Between each sector plate there are earthed screens, by which the electrical interaction between the sector plates are prevented. Above this rotating part the earthed metal case F with a sector shaped opening is covered, through this opening the sector plate can be exposed to the external electric field. H, I, J and F are always earthed. As shown in Fig. 3 (a), the surface of three sector plates and the upper edges of three intervenning screens are all in the same height, therefore in rotation these do not contact with the inner surface of the earthed case F, but maintain very narrow gap. This gap is so narrow that no lines of force can enter. Each plate A, A′, A″ has small metal disc C, C′, C″ with thin metal rod B, B′, B″. In Fig. 3 (a) D is a brush connected to the electrometer, this is a small metal wheel as shown in Fig. 3 (b). Small metal disc C comes in contact with the limb of this wheel without slipping, and rotates the wheel smoothly; by this the contact

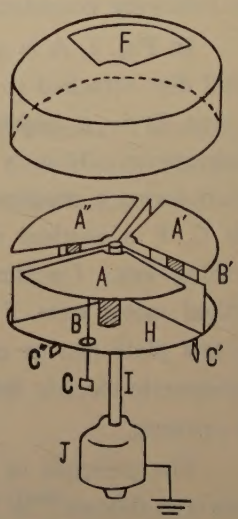


Fig. 2 Schematic view of the air-earth current collector

between the plate system and electrometer system is made. Both small metal disc C and small metal wheel D are made of same material, and thin metal rod B is somewhat flexible.

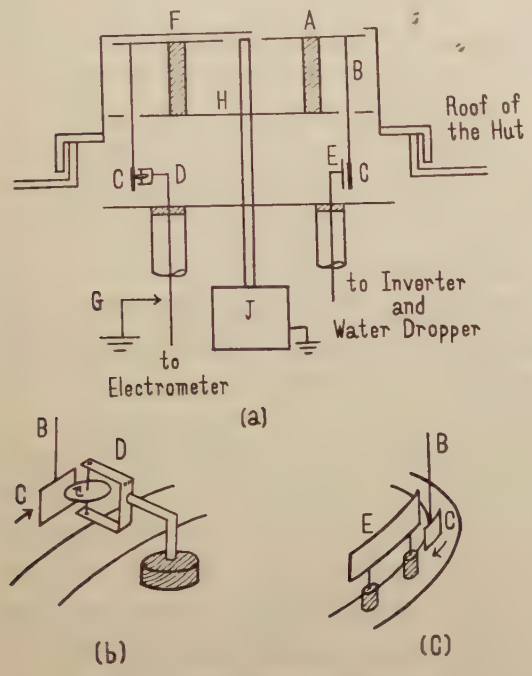


Fig. 3 Air-earth current collector

Whether any unfavourable disturbances occurs or not is examined in the unceasing contacts between C and D. An earthed cover plate is put on the opening of the case F, that is the system is rotating under the non electric field. It is ascertained that there is no deflection of the electrometer.

E in Fig. 3 (a) is a plate of the compensator, as shown in Fig. 3 (c). Metal disc C moves along E without touching, but maintainning a constant distance from it. In this condition C and E make a compensating condenser. In Fig. 3 (a) D and E are shielded from each other, therefore there is no interference between them. Preliminary test is carried out to ascertain the independency between the electrometer system and compensator by applying arbitrary potential to E artificially when the apparatus is in action.

In the case of our compensator, as shown in Fig. 4, the collector is employed instead of battery. As a collector, water dropper is employed in the present case. Water dropper acquires the net charge of the same sign as that of external field, therefore it is necessary to reverse the sign for the present purpose. As shown in Fig. 4, an inverter driven by motor is settled between water dropper and compensating condenser. This inverter has a function of reversing the sign and adjusting the magnitude of potential from the dropper, therefore charge which is just enough for compensation can be applied to E when the sector plate is exposed to the atmospheric electric field.

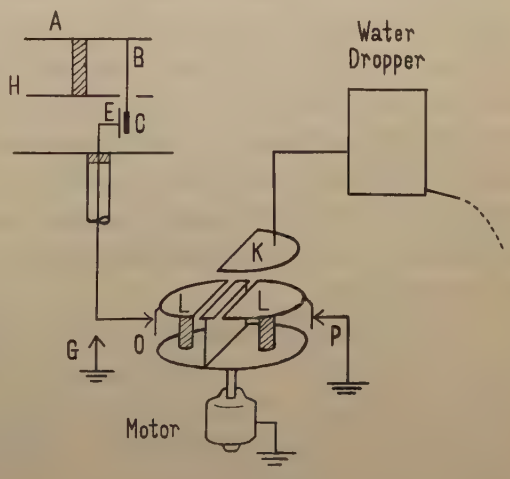


Fig. 4 Inverter

O and P are the brushes which contact with the brush wire fixed to the plate L; P is earthed, and O is connected to

compensator electrode E. This apparatus is shielded from the external electric field. Thus once adjusted, then the compensation is made automatically how the sign and the intensity of the external field may change.

Preliminary test whether the compensation is comple or not is made. It is expected that a little time lag may occur in this method of compensation when field changes rapidly, for the water dropper has a large equivalent resistance. Therefore the use of quick response collector is desirable. The number of revolution of the apparatus is usually 45 RPM or so. Any differences were not found in observation so far as the revolution is between 30 and 60 RPM. Thus potential of each sector plate system and the electrometer system rises by the charge from the air earth current without influence of the induction by atmospheric electric field.

The electric capacity of each sector plate system be $C_1$ (under the earthed cover) and the capacity of the electrometer system (small wheel, leading wire and the electrometer) be $C_0$, then the total capacity $C_t$ of the apparatus in action, is given as $C_t=3C_1+C_0$. In our apparatus $C_1=66\,\text{cm}$, $C_0=42\,\text{cm}$, therefore $C_t=240\,\text{cm}$.

It is very important to keep the insulators in a good condition. When there is a leakage through the insulator supporting the sector plate, this apparatus acts as an incomplete rotating collector of the agrimeter type, therefore air earth current measurement becomes impossible. For this reason the following means is made. Slow air stream, being previously dried by the absorbent, is supplied through a pipe around the surface of the insulator constantly; it is proved no serious trouble occured even in a moist weather.

The unit time change of atmospheric electric field (1 Volt/Meter/sec.) corresponds to the displacement current of $8.8\times10^{-16}\text{Amp/cm}^2$, which is about 4 times greater than the average value of air earth current. Such a small time change of field (1 per cent fluctuation of the field 100 Volt/Meter in a second) is not rare in the atmospheric electric field, so that the elimination of the induction is very important. Examination whether this apparatus suffers any kind of field induction or not is carried out by the following method. Above the apparatus the artificial electric field of arbitrary strength is impressed, that is stationary, impulsive and oscillatory. The impressed field amounts 10000 Volt/Meter or so. By the instantaneous reversal of the commutator switch the considerably large time change of field are also applied. In each examination it is confirmed that there are no deflection of the electrometer. Consequently this apparatus is able to be used in the observation under the rapidly changing electric field such as thunderstorm time.

The figures illustrated above are all simplified sake for easy understanding. The value of air earth current is deduced as follows. Let $i$ ($\text{Amp/cm}^2$) be the air earth current density, $A$ ($\text{cm}^2$) the area or a sector plate, $C_t$ (cm) the total capacity of the apparatus, $t$ (sec) the duration during which the system being insulated, $V$ (Volt) the potential increment of the system, then the following relation holds, $V=\frac{9\times10^{11}iAt}{C_t}$. In our sector plate apparatus, $A=194\,\text{cm}^2$, $C_t=240\,\text{cm}$, $t=100\,\text{sec}$. The system is insulated during 100 sec, and earthed 20 sec by the earthing key $G$, therefore the

observation is carried out cyclic every 2 minutes. In order to acquire large $V$ for given $i$ and $t$, the ratio $A/C_t$ of the apparatus must be large. $A$ and $C_t$ becomes larger as the dimension of the apparatus becomes larger, therefore the ratio may have a certain limit. In the apparatus of F.J. Scrase (1933) $A=8281\ \mathrm{cm}^2$, $C_t=3850$ cm, therefore $A/C_t=2.15$ cm. In ours $A/C_t=0.8$ cm, the Scrase's apparatus is effective than ours in this point of view.

The sensibility of our quadrant electrometer is of the order of $10^{-3}$ Volt/mm on the photographic paper, so that the air earth current can be measured by the drift method. Just after the earthing has finished, the potential of the sector plate system rises from zero by the charge from the air earth current. The field induction on the sector plate when exposed to external electric field is compensated by the compensator, but the potential increment by air earth current is not compensated, therefore excessive large increment may distort the field above the apparatus. Scrase (1933) noticed that in the drift method the field distortion will be negligible, provided the potential increment of the test plate is less than 0.25 Volt. Therefore in our apparatus the system must be earthed to zero potential, before the potential increment grows too much. As the time duration of insuration is 100 sec, potential rises are always within above limitation.

By slight modification of the apparatus, the precipitation current can be measured without suffering from field induction.

Instead of sector plate the sector trays are used, the bottom of which the woolly cloth is spread sake for the prevention of the raindrop splashing. In this apparatus the compensator is unnecessary. It is thought that in the case of small precipitation current and yet large field change, the existing exposed vessel type of precipitation apparatus may give some error.

### 3. Observations

Air earth current (by sector plate apparatus) together with atmospheric electric field (by rotating collector of the agrimeter type) is registered on the same photographic paper. For the registration of the air earth current, the light source of the electrometer is extinguished at the time of earthing, so that the departure from zero potential just after the beginning of the insulation can be observed distinctly. The period of the quadrant electrometer for the registration of potential gradient is 2.5 sec. The running speed of the photographic paper can be adjusted in a wide range by regulating the

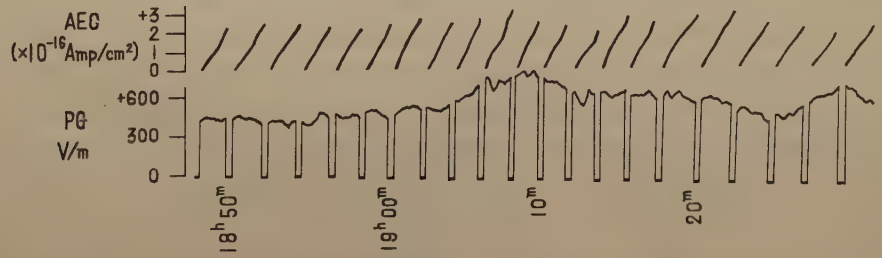


Fig. 5 (a) Fair-weather record, Apr. 3, 1957

mechanism attached to the recorder as one pleases.

The observation hut is situated on the top of the small mountain, 568 meters. above the sea level, near Mt. Aso. Both air earth current apparatus and rotating collector are situated on the roof of the hut side by side.

Typical examples of the records are shown in Fig. 5 (a), Fig. 5 (b) and Fig. 5 (c). Fig. 5 (a) is the record in fair weather when the electric field is comparatively changing. The ordinate scale value of air earth current record means that the height of the end point of the image drift gives the mean current density during 100 second. The ordinate scale values of both air earth current and electric field are not yet reduced to plain values, these are values in actual place. The actual values of potential gradient are estimated from the calibration by applying artificial electric field of known intensity upon the rotating collector.

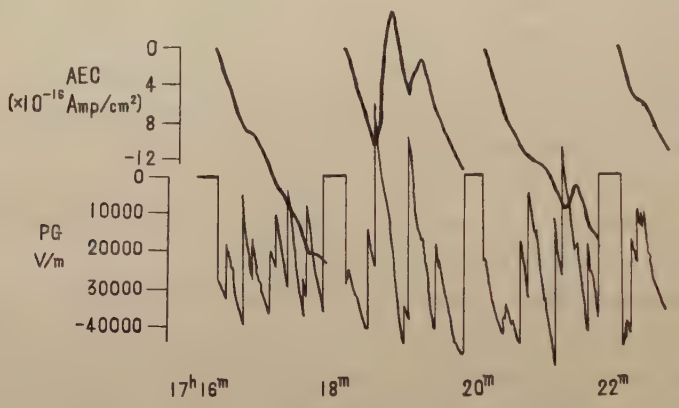


Fig. 5 (b) Thunderstorm record, Aug. 26, 1957

Fig 5 (b) is the record at the time when active thundercloud is approaching gradually, but precipitation does not yet begin. Many lightning discharges are found in the potential gradient record. The rainfall began about 10 minutes after the end of this recording. The period of the quadrant electrometer employed for air earth current registration is 20 sec, so that the deflection of electrometer for the air earth current can hardly follow the rapid changes accompanying lightning discharges. It is desirable to use more quick response one. In this record potential gradient shows many sudden changes due to lighnting discharges. The sudden changes are almost in the range of negative electric field, but very short time interval potential gradient reverses its sign from negative to positive occasionally. The magnitude of the positive air earth current in such a momentary positive electric field amounts considerably larger than the negative air earth current in such a continuing negative electric field. Under the sudden field changes by lightning discharges, it is presumed that the conductivity of the atmosphere, that is, the density and distribution of the positive and negative ions are apt to be in abnormal state. Concerning this point more detailed investigation is desirable.

Fig. 5 (c) is the record just before the above record. In this case there is no

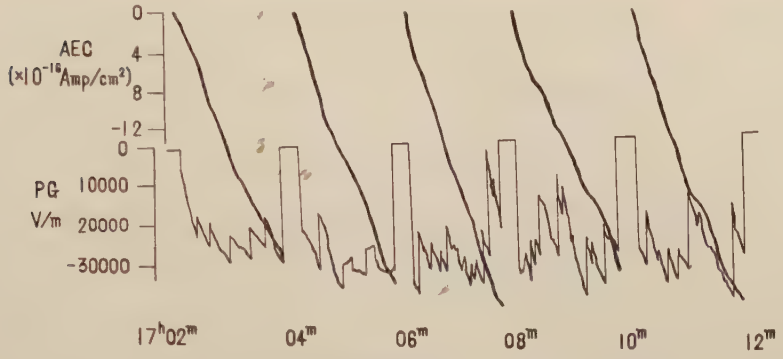


Fig. 5 (c) Thunderstorm record, Aug. 26, 1957

reversal of sign in the potential gradient. Both average values, not reduced to plane surface, of potential gradient and air earch current density in this case can be estimated as 30000 Volt/Meter and $3\times10^{-15}$ Amp/cm$^2$ respectively. Comparing these values with the average values in fair weather, that is 500 Volt/Meter and $3\times10^{16}$ Amp/cm$^2$ from gross estimate, the ratio between them are found to be 60 for potential gradient and 10 for air earth current density. This means that in high potential gradient the air earth current probably approaches to a saturation value. Attending to the fact that the slow response of the quadrant electrometer and the time lag in the compensator caused by the tardy water dropper make difficulties in the observation of rapidly varying air earth current, the above discussions must be reexamined. More quick response electrometer and more rapid working compensator are now preparing in our laboratory.

## 4. Acknowledgement

The author wishes to express his gratitude to Prof. Y. Tamura and Dr. H. Hatakeyama for their guidance, encouragement and discussions.

## References

[1] C.T.R. Wilson, 1905 Proc. Camb. Phil. Soc. **13**, 184–189; 1906 Proc. Camb. Phil. Soc. **13**, 363–382; 1908 Proc. Roy. Soc. (A) **89**, 537–547.

[2] E.J. Scrase, 1933 Met. Office. Geophys. Mem. No. 58.

# Magnetism of the Earth Crust

By Naoto KAWAI

*Geological and Mineralogical Institute, Kyoto University, Japan*
(Read May 12, 1957; Received Dec. 1, 1957)

**Abstract**

In Part 1 the present writer proposes a method by which the pressure and temperature conditions under which rocks have been formed can be clarified from mesurements of magnetic state of rock-forming minerals. The method is established by being based upon observations of piezo-thermal equilibria of titaniferous ferrites and silicates which are prevailing in the lithosphere.

In Part 2 is described the details of the method mentioned above.

In Parts 3 and 4 are discussed the following subjects:

1) Zone of titaniferous ferrite in the crust,
2) Separation of the crust into three magnetically different layers; namely the uppermost layer of ferromagnetism due to ferrite, the middle layer of paramagnetism due to titaniferous ferrites and the lowest layer of paramagnetism without titaniferous ferrites,
3) Region of thermo-remanent magnetism,
4) Composition and Curie point of ferrite as the indicator of the depth at which plutonic rocks were formed initially.

## Introduction

When magnetic measurements are made on plutonic rocks taken at the earth's surface, the results of these measurements will yield informations about the nature of magnetism that the subsurface material possesses; the plutonic rocks must have originated at great depths in the earth's crust and at present remain in themselves relics of magnetism which have been formed under high temperatures and high pressures prevailing there. Therefore, from measurements on these relics the magnetism existings in these great depths may be inferred.

Likewise, measurements on magnetism of varied igneous rocks and altered sediments may be utilized to account for the magnetic characteristic of the portion of the crust where the so-called metamorphism took place.

Magnetism of volcanic and sedimentary rocks may be seen as records of the geomagnetism in a remote past, but on the other hand may be a relic by which the magnetic state of the uppermost part of the lithosphere can be inferred. Measurements of magnetism of volcanic and sedimentary rocks will enable us to estimate the condition under which these rocks were formed and their magnetism appeared.

In the light of the above-mentioned line of thought, the experimental data the present writer obtained of a number of samples of plutonic, metamorphic and volcanic rocks have been arranged and the following qualitative results are obtained :

1) Curie point and intensity of remanent magnetism of plutonic rocks decrease with increasing depth at which they were originally formed,
2) Those of metomorphic rocks also decrease with increasing grade of metamorphism,
3) Those of volcanic rocks also decrease with increasing temperature at which they solidified.

In order to confirm the above-mentioned qualitative results in a quantitative way, the present writer carried out laboratory experiments to find how Curie point and remanent magnetism of various rocks change with varying pressure and temperature. The highest limit of the pressure the experiment has attained is 19,000 atm and that of temperature 700°C. The rock sample exployed for these experiments is $(10\times10\times2)$ $mm^3$ or $(\pi\times4\times4\times2)$ $mm^3$. The kinds of rocks used for these experiments cover almost all the rocks employed for the deduction of the above-mentioned qualitative results.

## Part 1 Natural occurrence of magnetic mineral as an indication of condition under which various kinds of rocks were formed

### § 1.1 Measurements on plutonic and metamorphic rocks

More than 1000 oriented and non-oriented samples of plutonic rocks have been collected from the so-called Ryoke zone and some other places in Japan. About 300 specimens of moderately or intensely modified igneous rocks and altered sediments have been collected from the well-defined suite of Ryoke and Sambagawa series in Japan, and also from the geosynclinal products of Tethys in Karakorum, Central Asia.

Besides the usual measurements of remanent magnetism thermo-magnetic observations and identification of ferromagnetic minerals, all these samples were subjected to paramagnetic susceptibility determination, from which number of atoms contained in 1 $cm^3$ of each rock sample was determined. The followings are the brief summaries of the results obtained from all the measurements mentioned above.

a) Comparison of remanent magnetism of the volcanic, plutonic and metamorphic rocks

In contrast to volcanic rocks which have strong ferromagnetism metamorphic rocks generally have so weak magnetism that even a resonance type magnetometer[1] can hardly detect it. Although there exist some exceptions* which have strong

* These samples of metamorphic rocks have been subjected to directed pressures under the geomagnetic field. The results indicate that the magnetism the samples possess prior to press seems to have been attributed to an effect of a directed pressure which applied to these metamorphic rocks during and after their formation. If a directed pressure is applied to a ferromagnetic material having a positive magnetostriction coefficient in such a way that the resulting magnetostriction energy overcomes the crystalline anisotropic energy or demagnetizing energy due to the material shape, there appears magnetization in the direction perpendicular to that of the pressure and parallel to the geomagnetic field. And even after the pressure is released, certain amounts of magnetism thus acquired remain as a kind of remanence. This remanence is called by Domen and the present writer " piezo-remanence ".

magnetism, it may be said that in metamorphic rocks the remanent magnetism is generally absent.

From the results of thermo-magnetic experiments, it is revealed that susceptibility of many metamorphic rocks is inversely proportional to temperature and satisfies the well-known Curie-Weiss' law, and therefore that their magnetism is paramagnetic.

Experiments on plutonic rocks show that their magnetism is intermediate or transitional between those of volcanic and metamorphic rocks. That is, nearly one half of the specimens of these rocks has remanent magnetism whose intensity is moderate and the other half has no remanent magnetism. Nearly all of the specimens shows a thermo-magnetic curve which is a superposition of a paramagnetic curve (a hyperbolic $\chi$-T curve) and a ferromagnetic.

The magnetic characters of these rocks are summarized in Table I.

Table I

| | Volcanic rocks | Plutonic rocks | Metamorphic rocks |
|---|---|---|---|
| Magnetic state of mineral | ferromagnetic | transitional from ferro- to paramagnetic | paramagnetic |
| Remanent magnetism | strong | moderate | almost zero |
| Intensity of remanent magnetism per gram | $189\times10^{-5}$ (e.m.u/gr) average of 436 specimens | $11.2\times10^{-5}$ (e.m.u/gr) average of 372 specimens | |
| Number of magnetic atoms in % | 5.41 | 4.48 | 4.30 |

b) Numbers of magnetic atoms (or ions) in 1 $cm^3$ of the three kinds of rocks and the seat of magnetic atoms in nature

Paramagnetic susceptibility of rock samples was determined from measurements at temperatures above their Curie or Néel points. By putting the thus obtained susceptibilities into the Curie-Weiss' formula, numbers of magnetic atoms in 1 $cm^3$ of the rock samples were calculated.

And it was found that despite the appearance of magnetism strikingly different from one to the other, the numbers of the magnetic atoms per 1 $cm^3$ of the samples were found nearly the same for the three kinds of rocks.

The average values of these numbers are 5.41, 4.48 and 4.30 atomic % respectively for volcanic, metamorphic and plutonic rocks as shown in Table I. These values show a fair agreement with the Clarke number 5.05% of Fe atom in the earth crust.

Since in the crust-forming rocks iron is regarded as the most abundant magnetic atom, such an occurrence of the various magnetic characters in nature as shown in Table I may be said to be due to the manner in which the iron atoms took their seats in the minerals during and after the rocks were formed; in other words, due to the circumstances in what mineral and in what proportions the iron atoms were accomodated.

It may therefore be said that the measurement of the magnetism of rocks is equivalent to that we have long been looking for the seat of the iron atoms in nature.

c) Occurrence of titaniferous ferrite in the three kinds of rocks

By means of X-ray, thermo-magnetic analyses and microscopic observation, further studies were undertaken. From these further studies it was found that ferromagnetic minerals responsible or not responsible for the remanent magnetism and those responsible for the paramagnetism were identified as follows:

c. 1) In almost all the volcanic rocks which the present writer has investigated, ferromagnetic minerals (ferrites) are always detected. The ferrites which appear frequently in these rocks are the members of solid-solution between magnetite and ulvöspinel.

c. 2) In contrast to this, ferromagnetic minerals common in metamorphic rocks are intermediate members of solid-solution between hematite and ilmenite*, and they appear more frequently than titanomagnetite** does.

c. 3) In plutonic rocks, either magnetite-ulvöspinel or hematite-ilmenite solid-solution is regarded as stable ferrites, and occasionally the both kinds of solid-solutions coexist in the same rock.

c. 4) The state of things mentioned in c. 1), c. 2) and c. 3) will be described in the following more in detail. In volcanic rocks, magnetite accompanies the eruption having taken place at very low temperatures and ulvöspinel does at very high, while titanomagnetites do at the intermediate temperatures. Hematite is an accessory mineral common in schists or semi-schists of very low grade of metamorphism, and ilmenite in those of very high, while the intermediate ferrites in moderately altered igneous and sedimentary rocks. In plutonic rocks, the two kinds of solid-solutions display a similar type of variations. Magnetite and hematite appear frequently in comparatively shallower portion of a batholith or in a laccolith, and ulvöspinel and ilmenite occur in a deep-seated mass, while the ferrites transitional between the two terminals of each solid-solution can be found in rocks moderately deep-seated.

c. 5) The above-mentioned may be summarized as follows: The Ti- contents in the two kinds of solid-solutions increase with rise of solidification temperature, with the progress of metamorphism, and with the depth of rock formation.

c. 6) To be noticed is that several specimens of most intensely modified rocks and of some igneous bodies which are considered to have been formed at great depths in the Ryoke geosyncline contain no trace of iron-titanium ferrites. This important fact has been confirmed by microscopic observation on thin sections of these specimens and also by thermo-magnetic identifications. The only magnetism we can observe in these specimens is the paramagnetism due to Fe-bearing silicate mineral in them. Nevertheless, numbers of magnetic ions per 1 $cm^3$ of these rock specimens, of which existence

---

*, ** Many authors have reported investigations on the magnetite-ulvöspinel and hematite-ilmenite solid-solutions. For instance, Pouillard[2] is the first to have introduced magnetic method of investigation and confirmed the regions in which each solid-solution is continuous. Nagata and Akimoto[3] have observed in detail the occurrence of these ferrites in volcanic rocks and studied the role they play in rock-magnetism, and Buddington and Balsely[4] did the same role in metamorphic rocks. While, Kawai, Sasajima and Kume[5] have confirmed the solvus relations these solutions display and studied their significance in rock-magnetism.

has been proved by observing temperature dependency of susceptibility, are nearly equal to the average number of the same ions which the present writer determined for all other specimens having spontaneous magnetism.

It may be plausible to interprete the above-mentioned facts as follows: If ferrites, which have become thus more and more Ti-rich as pressure and temperature increase, are further subjected to extremely high pressures or temperatures or both, they at last vanish and change into a kind of Fe-bearing titaniferous silicates which are entirely paramagnetic.

§ 1.2 Laboratory examinations under high pressures and temperatures

In order to confirm the conclusions obtained and described in the preceeding setion, § 1.1, temperature and pressure dependencies of the stability of the ferrites were examined in laboratory by using an apparatus as shown in Fig. 1. Fig. 1 (A) shows the pressure generating equipment and Figs. 1 (C) and (D) the vessels of which in a hole of a cylindrical or cubic form a sample is placed and submitted to a hydrostatic pressure. By using an electric furnace F in which the vessel is placed, temperature of the specimen can be raised up to about 700°C. To make the pressure in the vessel as hydrostatic as possible, a small quantity of water was put into the hole of the vessel and was employed as a pressure transmitting medium. Leakage of the vapour (the employed temperatures are over 300°C) out of the vessel is prevented by means of copper packings which are sandwiched between the vessel and the piston at their contact plane (see Fig. 1 (D)).

Inner part of the vessel is made of sapphire or tungsten carbide of which along the central axis is made the hole mentioned above and the piston of tungsten carbide, both of them being surrounded by stainless steel blocks to protect them from fracturing during the experiments (Figs. 1 (C) and (D)).

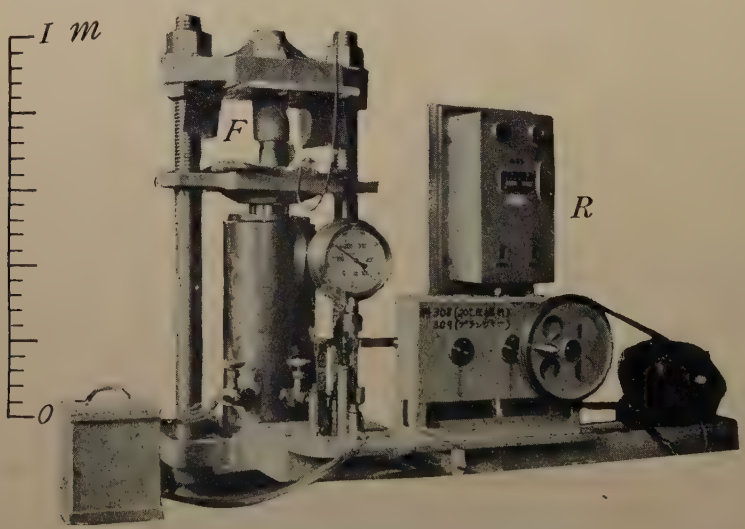


Fig. 1 (A) Pressure generating equipment
F: Electric furnace
R: Automatic pressure regulator

Fig. 1 (B) Buffer


Fig. 1 (C) Sapphire vessel
S: Sapphire
st: Stainless steel
h: Electric heater
j: Hole for thermo-couple


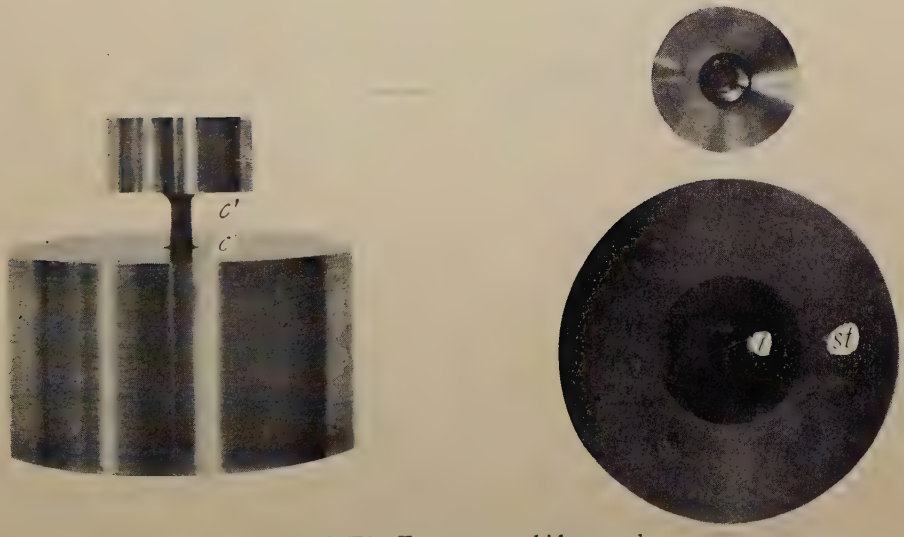


Fig. 1 (D) Tungsten carbide vessel
c, c': Contact planes of piston and vessel, copper packing is sandwiched between c and c'
t: Tungsten carbide
st: Stainless steel

The sample to be charged into the hole of the vessel is in a form of circular or cubic thin plate 2 mm thick and the size of the basal section $(10\times10)\,mm^2$ or $(\pi\times4\times4)\,mm^2$ just fits the cross section of the hole.

The period of time during which the sample is submitted to a given high temperature and high pressure is made to be more than 100 hours.

After the experiment the sample is quenched and taken out of the vessel and thermo-magnetic measurement is done.

This procedure is repeated for each of a number of combinations of high pressures and high temperatures. When we can infer from the series of the thermo-magnetic curves thus obtained that mass of one ferrite phase is growing with time, then we assume that this ferrite has been in equilibrium with and therefore stable at each of the combinations of the high temperatures and pressures. In these phase analyses the thermo-magnetic curves are made to be referred to the Curie and Néel points of the titaniferous ferrites vs the composition relations which have preliminally been obtained by Kume[7] for the rhombohedral ferrite, and also by Kawai, Sasajima and Kume[5] for the cubic ferrites.

When the temperatures are higher than 700°C, the piston and the vessel undergo extreme deformation making the experiment almost unable. And when experiment is made at temperatures lower than 300°C, it occurs that owing to the sluggishness of atomic diffusion, complete attainment of the equilibrium state requires an extremely long time, and at the same time owing to large hysteresis of solid-phase transformations, both the temperature and pressure corresponding to an equilibrium state is apt to be over or lower estimated. The experiments at temperatures higher than 700°C and lower than 300°C are, therefore, put beyond our experimental technique. Consequently, three runs of experiments were carried out at temperatures 350°C, 400°C and 550°C by simultaneously applying to each of these temperatures a series of hydrostatic pressures 2000, 4000 and 15000 atm.

The results obtained by the experiments are described in the following:

Table II Results of experiments at high temperatures and pressures

| Pressure \ Temperature | 350°C | 400°C | 550°C |
|---|---|---|---|
| 2,000 atm | | IL-HE 48% θ=370°C | IL-HE 53% θ=350°C |
| | | UL-MG 20% θ=310°C | UL-MG 25% θ=395°C |
| 4,000 atm | IL-HE 53% θ=340°C | IL-HE 60% θ=290°C | UL-MG 55% θ=175°C |
| 6,000 atm | IL-HE 65% θ=235°C | UL-MG 65% θ=105°C | |
| | UL-MG 60% θ=135°C | | |
| 15,000 atm | | | vanishing of ferrite into silicate was observed |

IL-HE : $TiO_2FeO$-$Fe_2O_3$ solid-solution
UL-MG : $TiO_2 2(FeO)$-$Fe_3O_4$ solid-solution
% : Molecular percent of ilmenite or ulvöspinel
θ : Curie point of ferrite

Curie points of rock specimens decrease as either temperature or pressure applied to the charge is elevated. This fact indicate that high temperatures and high confined pressures render ferrites Ti-rich. This conclusion shows a fair agreement with one of the field evidences described previously.

The results of these experiments are given in Table II, in which Ti-contents and the Curie points of each equilibrium phase are tabulated with respect to each equilibrium condition.

## Part 2 Piezo-thermal phase diagram (P-T diagram) of titaniferous ferrites and the stability domain of rock kinds

### § 2.1 P-T diagram showing domain of rock kinds and distribution character of magnetic minerals

Natural states of ferrites, especially the correlations between their Ti-contents and the conditions under which the rocks bearing these ferrites have been formed are, as has been stated, so systematic that it is possible to draw a P-T diagram showing domains of the rock kinds.

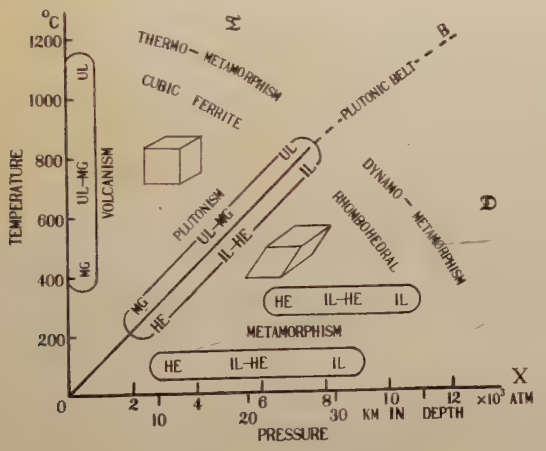


| | | |
|---|---|---|
| UL : | Ulvöspinel | $TiO_2 2(FeO)$ |
| MG : | Magnetite | $Fe_3O_4$ |
| IL : | Ilmenite | $TiO_2FeO$ |
| HE : | Hematite | $Fe_2O_3$ |
| UL-MG : | Solid-solution between magnetite and ulvöspinel | |
| IL-HE : | Solid-solution between hematite and ilmenite | |
| PS : | Paramagnetic silicate | |
| $\mathfrak{T}$ : | Domain of thermo-metamorphism | |
| $\mathfrak{D}$ : | Domain of dynamo-metamorphism | |

Fig. 2 Domains of rock kinds and of the ferrites therein

So far as known from many volcanologists' temperature evaluation, solidification of lava is found to have occurred in a comparatively broad range from 1300°C down to 400°C. Lava ejected over the surface of the earth's crust solidifies under the pressure far smaller than those under which plutonic and metamorphic rocks are formed. Therefore, domain of volcanic rocks can be shown schematically on the P-T diagram by a long elliptical area whose longer axis lies near and parallel to the temperature axis of the diagram.

As for metamorphic rocks the situation is quite opposite to that said above. For metamorphic rocks the temperature range is smaller and the pressure range greater than those of volcanic rocks. Therefore, the domain of metamorphic rocks is represented by an area enclosed by a ellipse whose longer axis is parallel to the pressure axis.

In the diagram a line OB is drawn in such a way that near the origin O the line bisects the angle between the temperature axis OY and the pressure axis OX. All points on this line will show the P-T conditions inside the lithosphere we are to encounter when we would descend in the earth crust vertically downwards. This line has been obtained from combination of the geothermal gradient in the upper portion of the crust and the gravitational load of the rock column. The P-T conditions on this line correspond to the ideal state of plutonic rocks or the normal state of the crust which involves neither thermo-metamorphism nor dynamo-metamorphism. The domain of plutonic rocks is, therefore, represented in the diagram by an elliptic area whose longer axis lies on the line OB. For convenience' sake, let us call the line OB "plutonic belt." Then this belt separates the whole area of P-T diagram into two sectors $\mathfrak{T}$ and $\mathfrak{D}$. If we take the P-T conditions on the plutonic belt as a standard, the temperature of any point inside the sector $\mathfrak{T}$ is greater than that of a point on the belt having the same pressure as that of the former point and the pressure of any point inside the sector $\mathfrak{D}$ is greater than that of a point on the belt having the same temperatures as that of the former point. Therefore, let us call the sector $\mathfrak{T}$ "the region of thermo-metamorphism" and $\mathfrak{D}$ "the region of dynamo-metamorphism."

Now let us arrange some of the most characteristic ferrites which have been mentioned in the field evidences given in Part 1 into the domains thus defined above. Bearing in mind the natural occurrences described in Part 1, (1) in the domain of volcanism, magnetite, titanomagnetite and ulvöspinel shall take their seats in the direction of increasing temperature as shown in Fig. 2. (2) in the domain of metamorphism, first hematite then hematite-ilmenite transitional ferrites and finally ilmenite in the direction of increasing pressure, (3) in the domain of plutonism, the arrangement

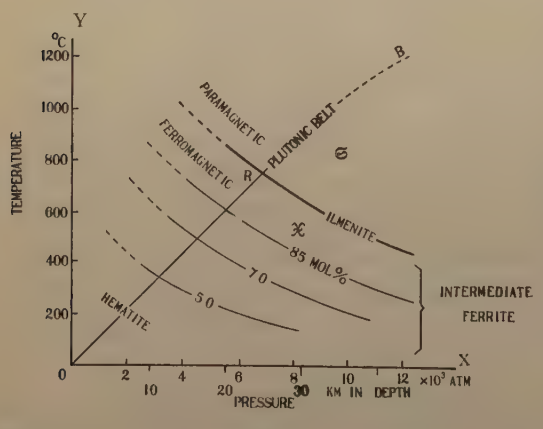


Fig. 3 (A) Stability diagram of rhombohedral ferrites compiled from combination of laboratory experiments and field evidences
% shows the molecular percent of ilmenite in the ferrites

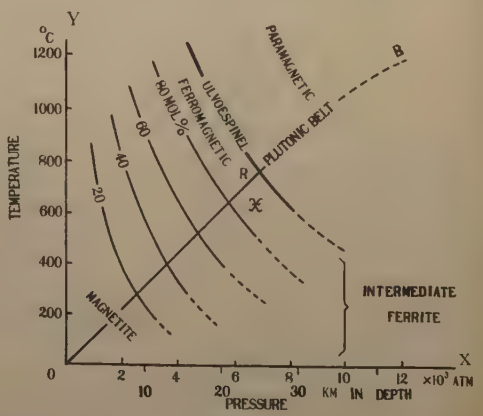


Fig. 3 (B) Stability diagram of cubic ferrites compiled from combination of laboratory experiments and field evidences
% shows the molecular percent of ulvöspinel in the ferrites

takes place in the order from Ti-poor to Ti-rich ferrite in the direction of increasing distance from the origin O, (4) in the sector $\mathfrak{T}$ of the thermo-metamorphism there prevail cubic ferrites (magnetite-ulvöspinel transitioal ferrite), and (5) in the sector $\mathfrak{D}$ of the dynamo-metamorphism rhombohedral ferrites (hematite-ilmenite transitional ferrites).

If the above proposed arrangements could tell us a true state of thing, it may be assumed that rocks having rhombohedral ferrites as accessory minerals have been subjected to dynamo-metamorphism, and that rocks having cubic ferrites to thermo-metamorphism.

§ 2.2 Pressure-temperature stability relation in both cubic and rhombohedral ferrites

If we intend to picture the P-T diagram by which both the natural occurrence and the laboratory experiments on both the cubic and rhombohedral ferrites could be plausibly explained, Fig. 3 (A) would be the diagram for rhombohedral ferrites and Fig. 3 (B) the cubic.

Buddington, Fahey and Vlisidis[6] have studied $TiO_2$ contained in ferrites from the data of chemical analyses and have published an idea that amount of $TiO_2$ in some magnetites is represented by an increasing function of temperature of the mineral formation.

But the present author's experiments indicate that Ti-contents in ferrites increase not only with increasing temperature but also with increasing pressure of mineral formation. Of this fact an explanation will be what follows:

If we assume that a very great hydrostatic pressure was applied to a rock and phase changes would associate in the rock forming minerals, then such phase changes are expected to be mostly of the type of volume-reducing changes, as such changes render PV energy of the rocks as a whole less. This expectation would imply in turn that the occurrence of such a type of phase changes would take place under high pressures.

It may be inferred that there are two kinds of process in which the total volume of the rock specimen is reduced under high pressures and simultaneously the Ti-contents in ferrites is increased. The first process is that in which Fe atoms contained in the ferrites are squeezed out and they are transported into the neighbouring silicates, so that the ferrite would become rich in Ti* and simultaneously undergo volume reduction and on the other hand the silicates, owing to their large capacity of accomodating Fe atoms, would not undergo such expansions that compensate the volume reduction of the ferrite. On further increasing pressure, Ti atoms in the ferrites begin to transfer into the silicates and the transference continues until at last the ferrites vanish. This change would be reversible. Silicates responsible for such a change can be considered as a condenser in which Fe and Ti atoms can be accomodated when pressure is increased and from which they can be expelled when pressure is decreased. This first kind of process is characterized by that silicate is a condenser for Fe and Ti and ferrite

* Rutile can occasionally be produced on the way of this transference of Fe from ilmenite to the neighbering silicate under high pressure.

a volume reducer. Many silicates such as pyroxene, hornblende, biotite etc play the condenser.

The second process is that in which the ferrites, instead of expelling Fe, absorb Ti atoms from the surrounding silicates under high pressures, and the resulting volume expansion of the ferrites is smaller than the volume contraction of the silicates.

This second kind of process is characterized by that silicate is a volume reducer and ferrite a condenser. One of the silicates playing the volume reducer is sphene found in many green rocks. Under increasing high pressure hematite becomes Ti-rich and tends toward ilmenite absorbing the Ti atoms from sphene. Ilmenite does vice versa in the reverse process under decreasing high pressure, expelling Ti atoms to produce sphene.

This phenomenon of the atom interchanges between the ferrites and the silicates is very interesting and seems to be important, and therefore now under a close examination.

**Part 3 Magnetism in the earth crust and the remanent magnetism**

§ 3.1 Stable zone of the solid-solutions in the earth crust

The stability curve of ilmenite and ulvöspinel shown by a heavy line in Fig. 3 separates the P-T diagram into two regions, of which one is the region $\mathfrak{X}$ bounded by the curve and the two axes, OX and OY, and contains the origin O and the other region the remaining region $\mathfrak{S}$. The region $\mathfrak{X}$ is the region in which ferrites can exist and the region $\mathfrak{S}$ that in which they cannot.

Let R (Fig. 3) denote the point of intersection of the line showing the plutonic belt OB and the boundary curve separating the $\mathfrak{X}$ and $\mathfrak{S}$ regions. The abscissa of the point R is about 6000 atm and corresponds to the depth of 25 km below the surface of the crust. Above this depth titaniferous ferrite exists and below this depth this oxide is absent. Therefore, if this is assumed to be true, we may infer that existence of minerals responsible for rock-magnetism is limited inside the uppermost shell of the earth, not more than 25 km or so in thickness.

It is also to be noticed that in iron oxides the distance from one iron atom to the neighbouring, being about 2Å, is so small that overlapping of the unpaired electron clouds, hence the molecular field, is likely to occur. And such a mineral is characterized by appearance of the spontaneous magnetism. Whereas in the silicate the iron atoms are widely spaced or otherwise are intercalated by a plane of the silicon-oxygen network, so that the exchange of the electrons is no longer possible, providing them with paramagnetism. Consequently the depth 25 km should also be regarded as the boundary above which the ferromagnetism exists and below which the paramagnetism does.

§ 3.2 Three magnetically different layers in the crust

The plutonic belt shown in Fig. 3 shows that Ti-content of the ferrites would increase with increasing depth. In consequence, Curie point whose value at the surface is about 600°C would decrease with increasing depth at a rate of about 40°C/km. On the contrary, if we assume a linear geothermal gradient of 30°C/km, the temperature

inside the crust whose surface value is about 0°C would increase with increasing depth at the above rate. Accordingly, there must be a certain depth at which the temperature of the crust would be equal to the Curie point of the ferrite prevailing there (Fig. 4). This critical depth, being graphically determined on the diagram in a manner as will be described later, will be about 10 km. In the outer shell from the surface down to this depth spontaneous magnetism, therefore, comes to existence due to the ferrites therein, because the temperatures inside this shell are always lower than their Curie points. Accordingly, the present writer calls this outer shell having a thickness of 10 km "ferromagnetic layer of the earth crust."

In the shell underlying the ferromagnetic layer extending down to a depth of 25km, temperature is always higher than the Curie points of the ferrites in this shell. Therefore, magnetism of this shell is always paramagnetic, despite of the existence of ferromagnetic materials. As we have demonstrated in the preceding section §3.1 paramagnetism without titaniferous ferrite is prevailing in the interior below the depth of 25 km. Accordingly, we can divide the earth crust into the following three magnetically different layers, namely the ferromagnetic layer, the paramagnetic layer with ferrites and the paramagnetic layer without ferrites (Fig. 4).

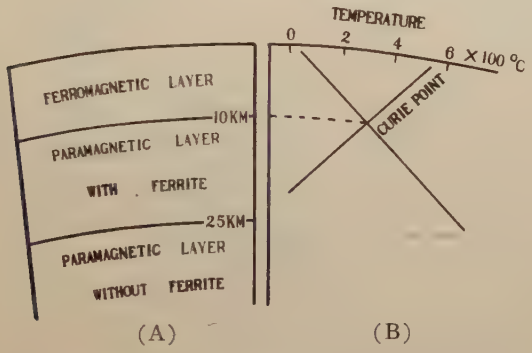


Fig. 4 (A) Three magnetically different layers in the crust

(B) Variation of Curie point of ferrite and temperature in the crust

§ 3.3 Region of thermo-remanent magnetism in the P-T diagram

Next to be clarified is the manner by which plutonic, metamorphic and volcanic rocks can acquire remanent magnetism. Figs. 5 and 6 are the diagramatical representation of the manner. Since there exists one to one correspondence between Curie point of ferrite and its composition, the five curves showing piezo-thermal stability relation shown in Fig. 3 can be regarded as the iso-Curie point curves.

If we draw on the diagram a line T=const., then this line intersects various iso-Curie point curves at various points, showing that even if temperature is held constant, the ferrites varying in Curie point can be formed according as pressure varies. Of these ferrites thus produced under various pressures with a constant temperature, one with its Curie point equal to T is represented by point P which is the intersection of the line T=const. and the iso-Curie point curve of T. Then it is evident that the ferrites lying on the line and on the left side of the point P have their Curie points all higher and those on the right side all lower than the temperature T at which the formation of these ferrites has taken place and their cooling has set in. So that these

ferrites falling on full lines of T=const. (Fig. 5) possess thermo-remanent magnetism (TRM), since they have been cooled passing through their Curie points, while those on broken lines possess no TRM.

By repeating similar consideration at various temperatures $T<T'<T''<T'''.....$, all the ferrites are classified into two kinds, of which one is capable and the other incapable of acquiring thermo-remanent magnetism. The domain of the former is represented on each of the two diagrams Figs. 6 (A) and 6 (B) by shadowed zone.

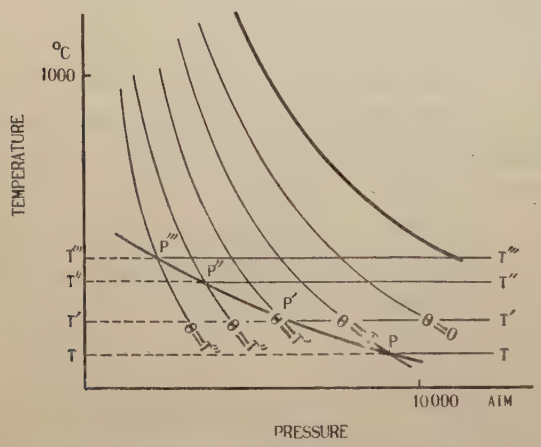


Fig. 5 Geometrical construction of region of thermo-remanent magnetism

Ferrites whose Curie points are lower than 0°C are paramagnetic at temperatures higher than 0°C and the rocks possessing these ferrites cannot be magnetized in the field and also in the laboratory unless they are being exposed to a temperature below 0°C, and therefore the area on the right side of the 0°C iso-Curie point Curve is not a TRM region in countries where the ground experiences no freezing.

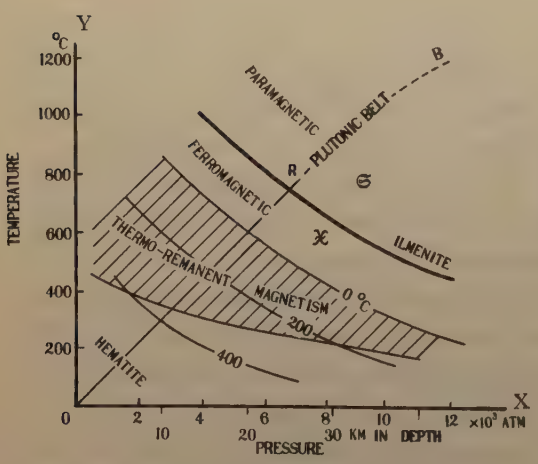


Fig. 6 (A) Region of thermo-remanent magnetism for $Fe_2O_3$-$TiFeO_3$ series

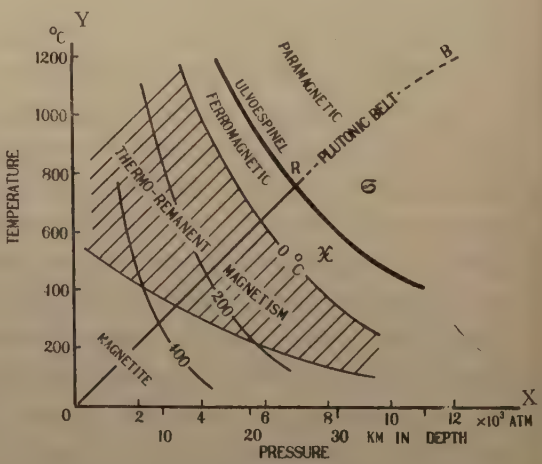


Fig. 6 (B) Region of thermo-remanent magnetism for $Fe_3O_4$-$TiO_2$2(FeO) series

Next, the specimens of volcanic, metamorphic and plutonic rocks which have been collected so far, totaling 1828, are classified into following three main groups, namely,

Table III

| Rocks | (A) | (B) | (C) | (B)+(C) | (A)+(B)+(C) |
|---|---|---|---|---|---|
| Volcanic rocks | 93.2% | 6.8% | 0.0% | 6.8% | 100% |
| Plutonic rocks | 17.8 | 42.5 | 39.7 | 82.2 | 100 |
| Metamorphic rocks | 15.7 | 21.0 | 63.3 | 84.3 | 100 |

(A) those having both remanent magnetism and ferrites, (B) those containing ferrites but without remanent magnetism, and (C) those having neither ferrites nor remanence. The relative proportions of the numbers of specimens in the three groups are tabulated in table III.

If the domains of three kinds of rocks shown in Fig. 2 and the shadowed area showing the region of TRM represented in Fig. 5 are compared with each other, one can find that the area common to the shadowed area and each domain is the greatest in volcanic, smallest in metamorphic, and intermediate in plutonic rocks respectively as shown in Fig. 7.

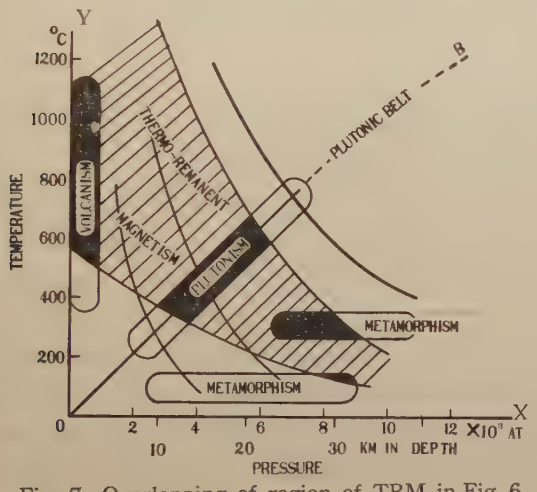


Fig. 7 Overlapping of region of TRM in Fig. 6 and three domains in Fig. 2

The numerals given in the column (A) of table III show a downward decrease from volcanic to metamorphic rocks and this is qualitatively consistent with what just has been mentioned for Fig. 7. This consistency would be plausible, if it could be assumed that the remanent magnetism in these rocks are thermo-remanent magnetism.

### § 3.4 Epoch of acquisition of thermo-remanent magnetism

It must be remembered that the plutonic rocks cropping out at the surface of the crust have cooled considerably and this cooling must have been affected by their upheaval and erosion away of their overlying rock strata. The upheaval must have been a slow movement caused by an isostatic readjustment or by a mountain making movement; hence it comes that the deeper the initial formation of the plutonic rocks and so the greater the upheaval and at the same time the lower the Curie point, the longer duration is required for the acquisition of the thermo-remanent magnetism. For instance, plutonic rocks which were made at 18 km depth from the surface and charged with ferrite of which the Curie point is expected to be about 100°C, should be left unmagnetized for long time until the rocks were lifted up to a level at a depth of 3 km below the surface. In fact, we occasionally find that some of the mesozoic plutonic rocks in Japan seems to have gotten their magnetism in tertiary period or even more recently, and further that the magnetization of these rocks is almost in the direction of the present earth's field,

despite of their remote origin. This retardation of magnetization should be taken into consideration for the palaeomagnetic interpretation of remanent magnetism of plutonic and metamorphic rocks.

**Part 4 Composition or Curie point of ferrite as the depth indicator of plutonic rocks**

It seems important to recall here the variation of Ti-contents in ferrite along the plutonic belt OB (see Fig. 2) and to consider its significance, because the composition of ferrite contained in a plutonic rock tells us the depth at which the rock was initially formed.

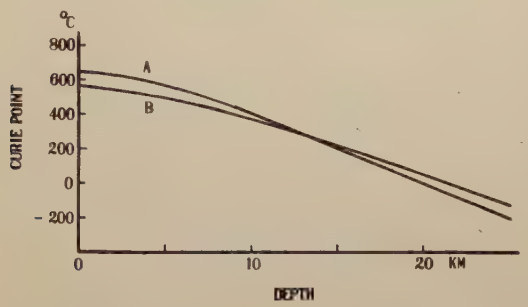


Fig. 8 Variation of Curie point of ferrite with depth

(A) For the series of solid-solution between hematite and ilmenite

(B) For the series of solid-solution between magnetite and ulvöspinel

In Fig. 8 are illustrated the relations of the depth *vs* the Ti-contents (or vs the Curie point), which have been drawn from Figs. 2 and 3.

If from a thermo-magnetic observation of a rock sample are determined its Curie points and also the composition of ferrite contained in it is determined by an X-ray analysis, one can infer from the curves in Fig. 8 at what depth the rock was initially formed.

The method of depth estimation mentioned above has been put into practice only very recently and of course quite tentatively, and therefore should be considered neither as an ultimate method nor as having generality valid for all cases. Nevertheless, some results of the depth estimations thus carried out encounter no conspicuous discord with geological field observations.

For instance, in the rock samples taken from various orogenic belts of the world at large such as Caredonia, Variscan, Alps, where mountain making movements and hence the land uplifts were conspicuous, we find paramagnetic or ferromagnetic ferrites of very large Ti-contents. In contrast to this, the samples of igneous masses from kratogens possess ferromagnetic ferrites whose Ti-contents are very small, regardless of the localities these rock samples were taken from and of their ages.

Granite and gabbro that have intruded into the Sinian system in northern Korea and in northern China, plutonic rocks in Ural (USSR), and Schwaltzwald (Germany) are the representative examples showing very high Curie points, that is, very low Ti-contents.

An interesting application of the above-stated depth-rule is given in the following: Granite samples were taken from outcrops at the summit 2900 m high above sea level and those at the foot 920 m high of Mt. Shirouma, Central Honshu, Japan which is

generally considered to be composed of same granite mass. The Curie point of the ferrite in the summit sample was found to be about 550°C and that of the ferrite in the foot sample 450°C, giving the difference in Curie points equal to 100°C. The difference expected from the depth-rule is about 80°C. The agreement between the observed and calculated difference is worth noticing.

A number of specimens of plutonic rocks from Japan and Karakorum were examined for depth estimation, giving the results shown in Table IV.

In the last, a remark should be given in the following on the application of the depth-rule. Plutonic rocks now cropping out at the earth's surface occasionally involve various kinds of ferrites, which have been made not originally but after the formation of the rock, all having been derived from it on a way decreasing temprature and pressure due to the upheaval. Such derived ferrites possess their Curie points all higher than that of the original, as has been already stated. Therefore, in case a number of different Curie points are found by thermo-magnetic analysis, the lowest Curie point is to be employed for the depth estimations. In finding the lowest Curie point, lower limit of temperature range for the thermo-magnetic analyses has been lowered to −196°C, the boiling temperature of nitrogen.

Table IV

| Specimen number and the locality | Depth estimated |
|---|---|
| 4211 (gabbro) Ryoke, Kinki | 12 km |
| 4201 (granite) Ryoke, Kinki | 18 km |
| 4550 (gabbro) Muroto, Shikoku | less than 5 km |
| M-106 (granite) Karakorum | 10 km |
| H-50 (granite) Rokko, Kinki | less than 4 km |

**Acknowledgements**

The author wishes to express his indeptness to Professor N. Kumagai for his constant interest and advice throughout the course of this work. He also wishes to thank Professor S. Matsushita, Professor A. Harumoto and Dr. H. Yoshizawa for the loan of their rock collections and for their valuable discussions. He is indebted to the late Emeritus Professor M. Matsuyama who gave him much encouragement throughout this study. Finally, he is indebted to the Grant in Aid for Fundamental Scientific Research of Ministry of Education for the finantial aid.

**References**

[1] Kumagai, N. and Kawai, N.: Memo. Coll. Sci. Kyoto Univ., Series B, 20, 307 (1953).
[2] Pouillard, E.: Ann. Chimie, 5, 164 (1950).

[3] Nagata, T. and Akimoto, S.: Geofi. pura Appl. Mirano, 34, 36 (1956).
[4] Balsley, J.R. and Buddington, A.F.: Jour. Geomag. Geoele., 6, 176 (1955).
[5] Kawai, N., Sasajima, S. and Kume, S.: Proc. Japan Acad., 30, 588, 864 (1954).
[6] Buddington, A.F., Fahey, J. and Vlisidis, A.: Amer. Jour. Sci., 253, 497 (1955).
[7] Kume, S.: Proc. Japan Acad., 31, 709 (1955).

# LETTERS TO THE EDITORS

## A Modification of the Method of E.R. Deutsch for the Magnetic Hysteresis of Rocks.


**Abstract**

Measurements have been made of the phase angle, $\phi$, by which the magnetic flux in a transformer core with an adjustable gap lags behind the 50 c.p.s. magnetising current. The lag is shown to be 3.5° for typical silicon steel laminations carrying an R.M.S. flux density of 600 to 2400 e.m.u. In the method of E.R. Deutsch [1] this lag is assumed to be zero, leading to errors in the hysteresis curves observed and an error $H_0 \sin\phi$ in the measured coercive forces, where $H_0$ is the amplitude of the magnetising field. It is concluded that the best method of obtaining a voltage proportional to the field in the gap of a magnet operated with alternating current is to use a search coil and an electronic integrating circuit.


### The Method of E.R. Deutch [1]

The method described by E.R. Deutsch uses a magnet built up of silicon steel laminations to provide an oscillating field of 50 cycles per second; the voltage across a resistance in series with the magnetising windings gives the horizontal deflection on an oscilloscope as a measure of the field in the magnet gap. The magnetisation of a specimen in the gap is determined differentially with a search coil, the signal in the absence of a specimen being reduced to a small value by connection in series opposition with another coli on one pole. With the minor addition of harmonic eliminating coils, the voltage from these balanced coils is displayed as the vertical deflection on the oscilloscope, giving a Lissajous-type figure. The difference in vertical deflection between the figures obtained with and without a specimen gives $dI/dt$ for the specimen, which is multiplied by $\frac{1}{\sqrt{1-\left(\frac{H}{H_0}\right)^2}}$ at each point to obtain $dI/dH$ and then $I$ by numerical integration.

It is essential to the method that the horizontal deflection of the oscilloscope beam be in phase with the measured field, since if the field, $H$, lags behind the magnetising current by a phase angle, $\phi$, $dI/dt$ will be advanced in the oscillograms by this angle and therefore by a fraction $2\sin\frac{\phi}{2}\cos\left(\frac{\phi}{2}+\sin^{-1}\frac{H}{H_0}\right)$ of the field amplitude $H_0$. Since we are interested principally in small values of $H/H_0$ and $\phi$ this means that there is an error $H_0\phi$ or $H_0\sin\phi$ in the field corresponding to each measured value of $\frac{dI}{dt}$.

In order to examine the magnitude of the error introduced by Deutsch's assumption that the phase lag, $\phi$, is zero, the lag was measured for two cores built up from silicon steel laminations of different sizes.

### Method of Measuring the Phase Lag of Magnetic Flux

The cores under examination were wound with large magnetising coils (200 to 2000 turns) and small secondary coils (1 to 10 turns) and connected into the circuit of Figure 1.

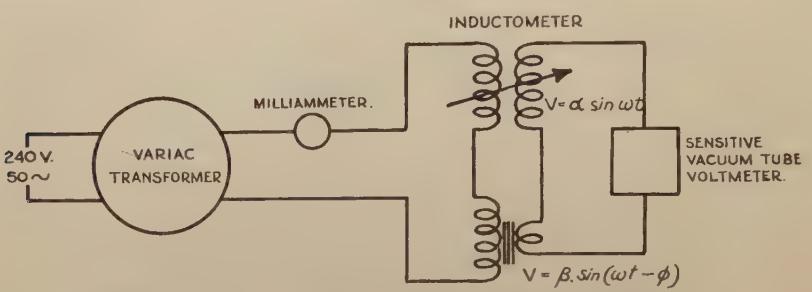


Fig. 1. Electrical Circuit for Phase Lag Measurements.

The method was essentially a comparison of the valtages induced in the secondary windings of a pure air-cored mutual inductance, for which a Cambridge Instrument Co. Campbell Mutual Inductometer was used, and the core under test.

The voltages may be represented as

$$\alpha \sin \omega t$$

and $\beta \sin(\omega t - \phi)$ respectively,

Where $\alpha$ and $\beta$ are arbitrary constants and $\phi$ is the phase angle to be determined.

The variable mutual inductance is first set to zero, so that $A=0$ and the amplitude, $V_1$, of the signal on the voltmeter is $\beta$.

The mutual inductance is then adjusted to give the minimum voltmeter reading. This voltage is

$$\begin{aligned} &\alpha \sin \omega t - \beta \sin(\omega t - \phi) \\ &= (\alpha - \beta \cos \phi) \sin \omega t + \beta \sin \phi \cos \omega t \end{aligned}$$

where $(\alpha - \beta \cos \phi)$ is adjusted to zero and the amplitude $V_2 = \beta \sin \phi$. Thus $\sin \phi$ is the ratio $V_2/V_1$ of the measured voltages.

The flux density $B$ in the core was measured as $iM/n_2 a$ where $i$ is the magnetising current, $M$ is the mutual inductance setting at balance, $n_2$ the number of secondary turns on the core of cross sectional area $a$. With $i$ in milliamperes and $M$ in millihenries this becomes $B = 100 \dfrac{iM}{n_2 a}$. Each test core was measured at a series of values of $B$ up to 3000 gauss R.M.S., more than covering the range used by Deutsch [1].

A number of transformer cores were examined, most attention being given to

two cores built up from silicon steel laminations of the same thickness, 0.056 cm., but different area. The air gaps were adjusted to reproduce approximately the same ratio, $\epsilon$, of reluctance of the air gap to total reluctance as that used by Deutsch [1], which is readily calculated from his figures:

Magnetizing windings of 2000 turns carrying 3 amperes gave a total magnetomotive force of 7539 oersted-cms. (R.M.S. value); the flux density 1700 gauss across a 3 cm. air gap gave an RMS magnetomotive force across the gap of 5100 oersted-cms., so that $\epsilon = 0.67_7$.

**Results of the Phase Lag Experiments**

The cores examined were:

(1) A commercial choke with a fixed air gap to which a secondary winding of two turns was added. This gave a phase lag varying between 19° and 32° depending upon the magnetising current.

(2) A spiral of permalloy tape 0.005 cm. thick with a total cross section of 1 sq. cm. was cut into two parts so that a variable air gap could be included in the magnetic circuit. With no air gap the core was used with a primary of 700 turns and a secondary of two turns and gave a phase lag of 13° at a flux density of 1000 e.m.u. increasing to 26° at flux density of 6,500 e.m.u. The addition of two 0.046 cm. thick air gaps required a primary winding of 3500 turns and a secondary of 10 turns. It reduced the phase lag to 1.2° at a flux density of 400 e.m.u. and 5° at 4,400 e.m.u. The inclusion of two 0.092 cm. gaps increased the phase lag to 3.5° at a flux density of 400 e.m.u. and 7° at 4000 e.m.u.. Owing to the high permeability of the core it was not convenient to use air gaps small enough to give a gap reluctance comparable with the yoke reluctance.

(3) A core was built from 0.056 cm. silicon steel laminations of standard transformer shape and with a central limb of width 3.175 cm. A sufficient number were used to make the cross-sectional area of the magnetic circuit 9 sq. cm. The core was used with a 2000 turns primary coil and three secondary coils of one turn each, closely wound on the central and two outer limbs of the transformer core, near to the "air" gaps. The secondary coils were connected in series so that their voltages added, and were effectively a single secondary coil of two turns, since the flux of the central limb of the core was shared between the two outer limbs. The precaution of winding the secondary coils in this manner was taken because the introduction of an "air" gap between the $E$ and 1 parts of the transformer core caused appreciable leakage flux, and the average flux across the gaps was required.

The components of the core were separated by a sheet of insulating cloth 0.020 cm. thick which gave $\epsilon = 0.65_8$ at $B = 1616$ gauss (R.M.S.).

The phase lag was about 3.5° almost independent of the flux density as indicated by the crosses in Figure 2.

To examine the effect of changing the size of the yoke while retaining the same lamination thickness, a second core was built up from 0.056 cm. silicon steel laminations

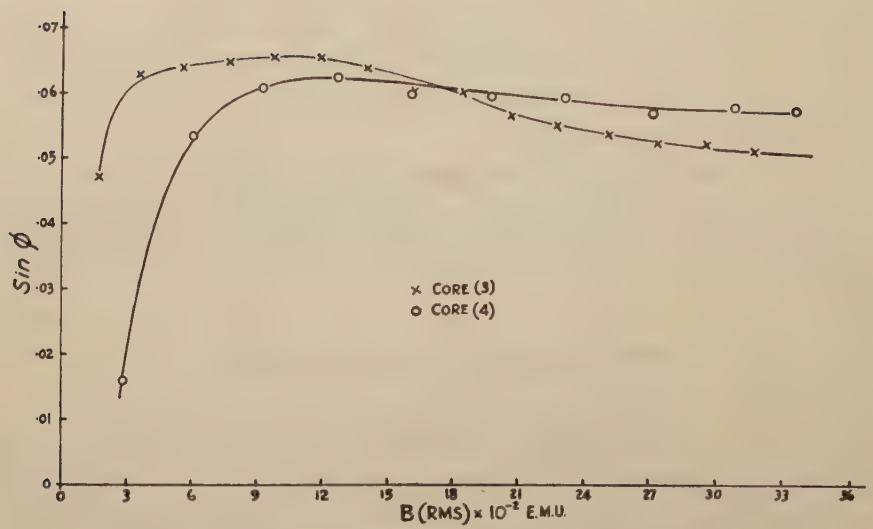


Fig. 2 Phase Lag of Magnet Flux vs. R.M.S Flux Density.

of standard shape but width 1.905 cm. of the central limb. This was used with a 1000 turns primary coil and three secondaries, wound as on core (3), and 0.013 cm. gaps between the $E$ and 1 components giving $\epsilon = 0.65_2$ at a flux density of 1613 gauss (R.M.S.).

The phase lag for this core, indicated by circles in Fig. 2, did not differ significantly from that observed with core (3) over the range of flux density of interest, 1000 to 2000 e.m.u. It is reasonable to assume that larger laminations of the same thickness operated with a gap reluctance equal to twice the yoke reluctance at 50 cycles per second would give a phase lag not greatly different from 3.5°. For a field amplitude of 2400 oersteds (1700 oersteds R.M.S.) this would introduce an error of 145 oersteds in the coercive forces measured by Deutsch's method and a corresponding distortion of other features of the hysteresis loops. The seriousness of this error can be seen from the results in Deutsch's second paper [2] which shows coersive forces of 100 to 200 oersteds.

## Modification of Deutsch's Method

In Deutsch's experiments the voltage from a resistance in series with the magnet windings was used for the horizontal deflection of an oscilloscope instead of the voltage from a coil over the field gap because a direct measure of the field and not a differentiation was required for display. If the field varied exactly sinusoidally the problem would be simple since a correction for the phase lag of the magnetic flux could be made during the numerical integration. Alternatively a search coil could be used with a differentiating circuit to produce a further phase change of 90°; the resulting voltage would be 180° out of phase with the magnet flux which would not be significant since hysteresis loops are symmetrical. To examine the second suggestion a circuit was set up to differentiate the voltage from the secondary coil on core (4) with the mutual inductometer, coupled to an amplifier which reduced the phase

change due to the inductometer reactance. The differentiation enhanced the third harmonic content of the search coil voltage producing a waveform quite unsuitable for use as a measure of the field. The strength of the harmonic content is such as to cause additional doubt about the use of the magnet current as a field measurement in Deutsch's method and leaves only integration of the search coil voltage as a reliable method of measuring the field. This can be accomplished automatically with a floating voltage source electronic integrator such as that indicated by Chance et al. [3] in Fig. 18. 34. With the addition of a cathode bias resistor this circuit can be made to integrate as accurately as the limitation on the resulting signal attenuation will allow. A similar circuit can also be used to integrate the signal from the balanced coils in Deutsch's method, giving oscillograms (with and without specimens) which are subtracted from one another to obtain hysteresis curves without numerical integration.

**References**

[1] Deutsch, E.R.: J. Geomag. Geoelect. 8, 108 (1956).
[2] Deutsch, E.R.: J. Geomag. Geoelect. 8, 118 (1956).
[3] Chance, B., Hughes, V., MacNichol, E.F., Sayre, D. and Williams, F.C.: Waveforms, M.I.T. Radiation Laboratory Series, No. 19, p. 663 (New York: McGraw-Hill 1949)

By F.D. STACEY and L.G. PARRY*

*Australian National University, Canberra, Australia.*

* On leave from New South Wales University of Technology, Sydney N.S.W.

# Positional Intermixing of the Normal and the Reverse Magnetizations of the Kawajiri-misaki Basalt Lavas

In this paper are reported the further results on the field observation of the Kawajiri-misaki basalt lavas as a supplement to the previous data. [1] From an area of one meter square of the outcrop belonging to entirely one rock block of the lavas, the present author has sampled further specimens, 17 in number, (from No. 27 to No. 43), in addition to 26 specimens already reported in the previous paper [1] and has reconfirmed the fact of the positional close intermixing of the normal and the reverse magnetizations in the very outcrop.

The arrangement of the whole 43 specimens old and new *in situ* which he has sampled is represented in Fig. 1.

Fig. 2 is the Wulff's projections of the directions of the natural remanent magnetism (N.R.M.) of these 43 specimens and in Table 1 are shown the numerical values of the directions and intensities of the N.R.M.

As can be seen from Fig. 2 and Table 1, the directions of magnetization are normal for 7 specimens of No. 3, 16, 28, 29, 30, 32, 33 and intermediate for the specimen of No. 31, while those are all reverse for the remaining 35 specimens. It is worth noticing that 7 specimens from No. 27 to No. 33 showing the positional close intermixing of the normal and the reverse N.R.M. possess very low intensity of magnetization of the order of magnitude of $(1\sim2)\times10^{-4}$c.g.s.e.m.u./g. and their directions of magnetization are nearly intermediate, deviating greatly from the direction parallel or anti-parallel to the present geomagnetic field. The above fact of the intermediate directions of the weak N.R.M. *in situ* seems to be the natural consequence of the self-reversal phenomenon, as the opposite magnetization produced by the self-reversal is not always exactly anti-parallel to the direction of the original magnetization having taken place prior to the self-reversal phenomenon. This field evidence suggests that

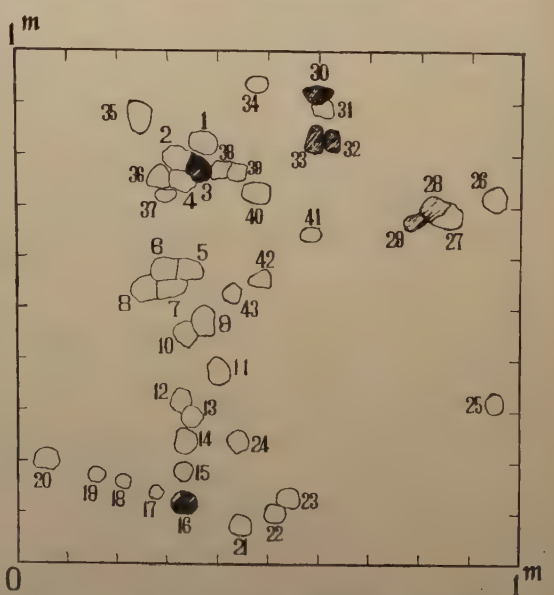


Fig. 1 The arrangement of 43 specimens sampled. No. 3, 16, 28, 29, 30, 32, 33 : normal
No. 31 : intermediate
The remaining 35 specimens : reverse


Fig. 2 Wulff's projections of the directions of the N.R.M. of 43 specimens. Big plots represent the lower hemisphere and thin the upper. The thick cross (×) indicates the direction of the present geomagnetic field.

Table 1 *Numerical values of the directions and intensities of the N.R.M. of 43 specimens. The intensities of magnetization are shown with the unit of* $10^{-4}$ *c.g.s.e.m.u./g.*

| Specimen No. | Declination | Dip | Intensity | Specimen No. | Declination | Dip | Intensity | Specimen No. | Declination | Dip | Intensity |
|---|---|---|---|---|---|---|---|---|---|---|---|
| 1 | +159° | −67° | 5.2 | ⑯ | + 52° | +29° | 4.0 | ㉛ | + 88° | −21° | 1.1 |
| 2 | +147 | −57 | 2.3 | 17 | +152 | −49 | 7.8 | ㉜ | + 25 | +26 | 2.1 |
| ③ | + 30 | +36 | 1.2 | 18 | +160 | −51 | 8.2 | ㉝ | + 51 | +12 | 2.1 |
| 4 | +159 | −55 | 5.1 | 19 | +173 | −53 | 9.5 | 34 | ±180 | −61 | 5.6 |
| 5 | +173 | −57 | 4.2 | 20 | +159 | −60 | 5.1 | 35 | +133 | −70 | 8.2 |
| 6 | +176 | −59 | 5.3 | 21 | −175 | −59 | 8.8 | 36 | +149 | −51 | 7.5 |
| 7 | −178 | −60 | 5.1 | 22 | +167 | −48 | 9.3 | 37 | +168 | −57 | 8.9 |
| 8 | −172 | −61 | 4.0 | 23 | −168 | −49 | 9.0 | 38 | +157 | −56 | 7.8 |
| 9 | +163 | −58 | 6.7 | 24 | +130 | −43 | 8.1 | 39 | +151 | −57 | 7.2 |
| 10 | +150 | −50 | 5.7 | 25 | +139 | −49 | 4.7 | 40 | +151 | −40 | 7.9 |
| 11 | +168 | −49 | 5.6 | 26 | +162 | −58 | 4.0 | 41 | +167 | −69 | 7.2 |
| 12 | +179 | −54 | 6.1 | 27 | +100 | −34 | 1.7 | 42 | +169 | −58 | 8.3 |
| 13 | ±180 | −59 | 6.5 | ㉘ | + 48 | +16 | 1.3 | 43 | −178 | −55 | 10.0 |
| 14 | +177 | −58 | 7.2 | ㉙ | + 24 | + 4 | 1.2 | The marks of circle (○): normal, square (□): intermediate. | | | |
| 15 | +171 | −66 | 6.7 | ㉚ | + 46 | +29 | 1.8 | | | | |

the author's interpretation stated in the previous paper [1] proves to be plausible.

The author is very grateful to Prof. N. Kumagai for valuable discussions and is also indebted to Messrs. T. Nakagawa and A. Miyazaki for helps in sampling the specimens from the field.

## Reference

[1] E. Asami: Journ. Geomag. Geoele., 8, 147 (1956).

Eizo ASAMI
*Department of Guidance, Kyoto University*

昭和33年3月20日　印刷
昭和33年3月25日　發行
**第9卷　第3號**

編輯兼發行者　日本地球電氣磁氣學會
代表者　長谷川万吉

印刷者　京都市南区上鳥羽唐戸町63
田中幾治郎

賣捌所　丸善株式會社京都支店
丸善株式會社 東京・大阪・名古屋・仙台・福岡

JOURNAL OF GEOMAGNETISM AND GEOELECTRICITY

Vol. IX No. 3

1957

# CONTENTS